Reducing Uncertainty in the Distribution of Hydrogeologic Units within Volcanic Composite Units of Pahute Mesa Using High-Resolution 3-D Resistivity Methods, Nevada Test Site, Nevada

By Brian D. Rodriguez, Don Sweetkind, and Bethany L. Burton

Open-File Report 2010–1304

U.S. Department of the Interior
U.S. Geological Survey

U.S. Department of the Interior
KEN SALAZAR, Secretary

U.S. Geological Survey
Marcia K. McNutt, Director

U.S. Geological Survey, Reston, Virginia 2010

For product and ordering information:
World Wide Web: *http://www.usgs.gov/pubprod*
Telephone: 1-888-ASK-USGS

For more information on the USGS—the Federal source for science about the Earth,
its natural and living resources, natural hazards, and the environment:
World Wide Web: *http://www.usgs.gov*
Telephone: 1-888-ASK-USGS

Prepared in cooperation with the U.S. Department of Energy, National Nuclear Security Administration Nevada Site Office, Office of Environmental Management under Interagency Agreement DE-AI52-07NV28100.

Suggested citation:
Rodriguez, B.D., Sweetkind, Don, and Burton, B.L., 2010, Reducing uncertainty in the distribution of hydrogeologic units within volcanic composite units of Pahute Mesa using high-resolution 3-D resistivity methods, Nevada Test Site, Nevada: U.S. Geological Survey Open-File Report 2010–1304, 498 p.

Contents

Appendixes

Figures

Tables

Conversion Factors

Inch/Pound to SI

Multiply	By	To obtain
	Length	
foot (ft)	0.3048	meter (m)
mile (mi)	1.609	kilometer (km)
mile, nautical (nmi)	1.852	kilometer (km)
yard (yd)	0.9144	meter (m)

SI to Inch/Pound

Multiply	By	To obtain
	Length	
meter (m)	3.281	foot (ft)
kilometer (km)	0.6214	mile (mi)
kilometer (km)	0.5400	mile, nautical (nmi)
meter (m)	1.094	yard (yd)

Vertical coordinate information is referenced to the 1866 Clarke Spheroid.
Horizontal coordinate information is referenced to the North American Datum of 1927 (NAD 27).
Elevation, as used in this report, refers to distance above the vertical datum.

Reducing Uncertainty in the Distribution of Hydrogeologic Units within Volcanic Composite Units of Pahute Mesa Using High-Resolution 3-D Resistivity Methods, Nevada Test Site, Nevada

By Brian D. Rodriguez, Don Sweetkind, and Bethany L. Burton

Introduction

The U.S. Department of Energy (DOE) and the National Nuclear Security Administration (NNSA) at their Nevada Site Office (NSO) are addressing groundwater contamination resulting from historical underground nuclear testing through the Environmental Management program and, in particular, the Underground Test Area (UGTA) project.

From 1951 to 1992, 828 underground nuclear tests were conducted at the Nevada Test Site (NTS) northwest of Las Vegas (DOE UGTA, 2003). Most of these tests were conducted hundreds of feet above the groundwater table; however, more than 200 of the tests were near, or within, the water table. This underground testing was limited to specific areas of the NTS including Pahute Mesa, Rainier Mesa/Shoshone Mountain, Frenchman Flat, and Yucca Flat.

Volcanic composite units make up much of the area within the Pahute Mesa Corrective Action Unit (CAU) at the NTS, Nevada. The extent of many of these volcanic composite units extends throughout and south of the primary areas of past underground testing at Pahute and Rainier Mesas. As situated, these units likely influence the rate and direction of groundwater flow and radionuclide transport. Currently, these units are poorly resolved in terms of their hydrologic properties introducing large uncertainties into current CAU-scale flow and transport models.

In 2007, the U.S. Geological Survey (USGS), in cooperation with DOE and NNSA-NSO acquired three-dimensional (3-D) tensor magnetotelluric data at the NTS in Area 20 of Pahute Mesa CAU. A total of 20 magnetotelluric recording stations were established at about 600-m spacing on a 3-D array and were tied to ER20-6 well and other nearby well control (fig. 1). The purpose of this survey was to determine if closely spaced 3-D resistivity measurements can be used to characterize the distribution of shallow (600- to 1,500-m-depth range) devitrified rhyolite lava-flow aquifers (LFA) and zeolitic tuff confining units (TCU) in areas of limited drill hole control on Pahute Mesa within the Calico Hills zeolitic volcanic composite unit (VCU), an important hydrostratigraphic unit in Area 20. The resistivity response was evaluated and compared with existing well data and hydrogeologic unit tops from the current Pahute Mesa framework model. In 2008, the USGS processed and inverted the magnetotelluric data into a 3-D resistivity model. We interpreted nine depth slices and four west-east profile cross sections of the 3-D resistivity inversion model. This report documents the geologic interpretation of the 3-D resistivity model.

Expectations are that spatial variations in the electrical properties of the Calico Hills zeolitic VCU can be detected and mapped with 3-D resistivity, and that these changes correlate to differences in rock permeability. With regard to LFA and TCU, electrical resistivity and permeability are typically

related. Tuff confining units will typically have low electrical resistivity and low permeability, whereas LFA will have higher electrical resistivity and zones of higher fracture-related permeability. If expectations are shown to be correct, the method can be utilized by the UGTA scientists to refine the hydrostratigraphic unit (HSU) framework in an effort to more accurately predict radionuclide transport away from test areas on Pahute and Rainier Mesas.

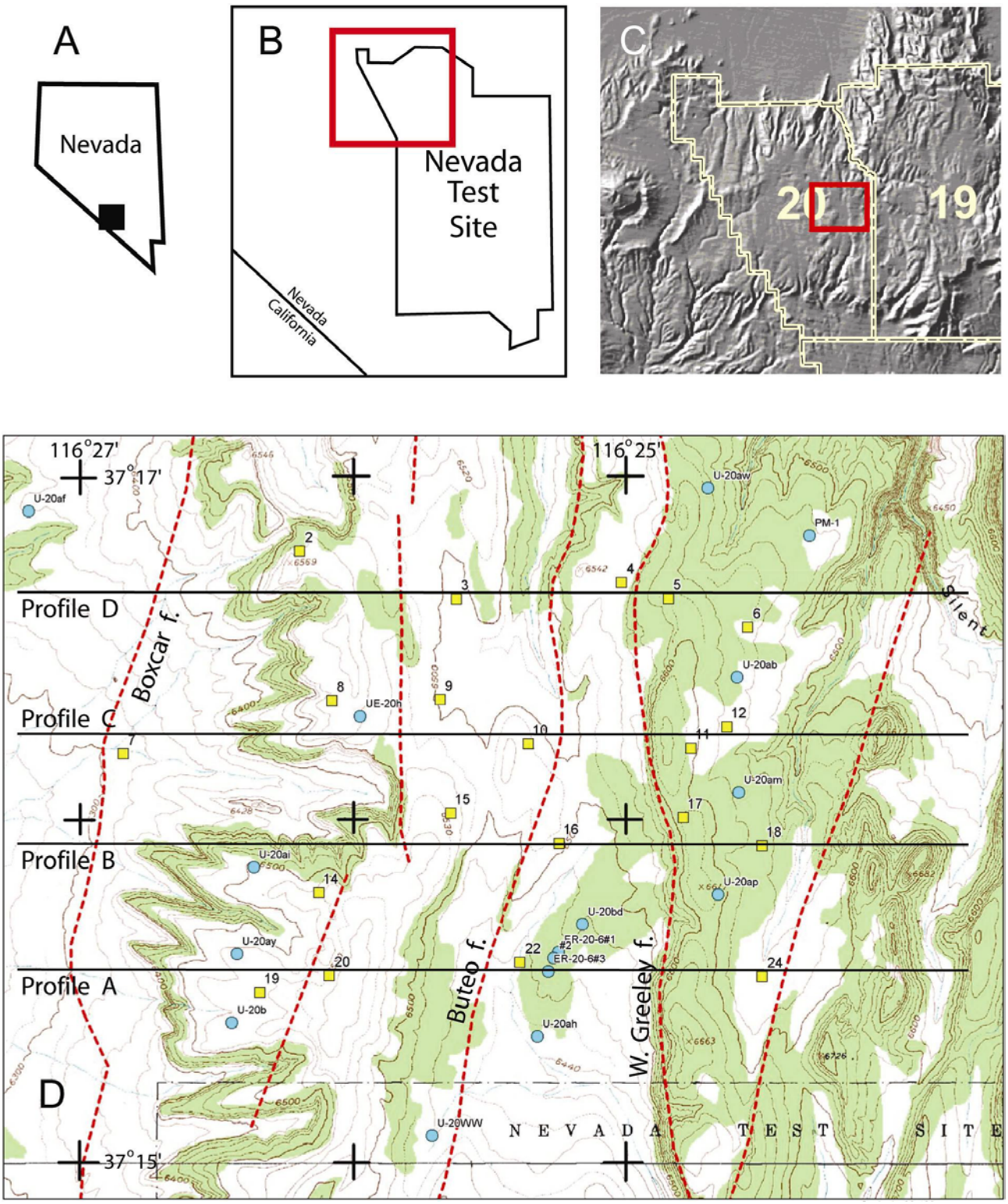

Figure 1. Profiles and magnetotelluric stations (yellow boxes), Area 20, Pahute Mesa, Nevada Test Site, Nevada. Base map from Silent Butte, Nevada, 1:24,000 topographic quadrangle. Blue circles are nuclear test drill holes or wells.

Geologic Background

The study area within the Pahute Mesa CAU is underlain by volcanic rocks of the southwestern Nevada volcanic field (SWNVF). The eruption of voluminous, regionally extensive ash-flow-tuff sheets occurred episodically from about 15.1 to 7.5 Ma and resulted in the collapse of at least six calderas (Byers and others, 1976b; Carr and others, 1986; Sawyer and others, 1994). The study area is within the Silent Canyon caldera complex, a composite caldera collapse structure resulting from the overlapping of Grouse Canyon and Area 20 calderas (Ferguson and others, 1994; Sawyer and others, 1994). This complex was subsequently buried by moderate thicknesses of ash-flow tuff erupted from younger calderas including the Claim Canyon caldera and the nested Rainier Mesa and Ammonia Tanks calderas (Byers and others, 1976a,b; Sawyer and others, 1994) to the south of the study area and the Black Mountain caldera to the northwest.

The volcanic deposits of the SWNVF consist of regionally extensive and large-volume ash-flow tuffs, numerous less extensive and smaller volume ash-flow tuffs, silicic lava flows and lava domes, fallout tephra deposits, and minor redeposited tuffaceous and epiclastic rocks (Byers and others, 1976b, 1989; Carr and others, 1986; Ferguson and others, 1994; Sawyer and others, 1994). Hydrostratigraphic units (HSUs) at the NTS have been grouped on the basis of similar geologic and hydraulic properties (Winograd and Thordarson, 1975; Laczniak and others, 1996; Bechtel Nevada, 2002, 2005, 2006; Faunt and others, 2004; National Security Technologies, LLC, 2007). These HSUs are based on volcanic rock type, such as lava flow and ash-flow tuff, and on physical properties, such as degree of welding and alteration (Laczniak and others, 1996). Outflow-tuff sheets, which make up many of the volcanic aquifers at the NTS, are regionally distributed and typically have well-connected fracture networks and minimal secondary alteration (Blankennagel and Weir, 1973). Fractured rhyolite lava flows and vitric ash-fall tuffs also are typically classified as volcanic-rock aquifers, but are relatively restricted areally (Prothro and Drellack, 1997). Zeolitically altered and nonwelded tuffs form important local confining units (Blankennagel and Weir, 1973; Winograd and Thordarson, 1975). Certain volcanic rock sequences are difficult to classify either as an aquifer or a confining unit because of heterogeneity and are referred to as volcanic composite units (VCU) (Prothro and Drellack, 1997; Bechtel Nevada, 2002).

The upper 600-m subsurface geology beneath the Pahute Mesa CAU is well-constrained by numerous wells that have been drilled to better characterize the geology and hydrology of the subsurface environment. Geologic data attained from these wells, and insights gained from surficial geologic mapping and other geologic investigations, have been integrated spatially to create 3-D hydrostratigraphic framework models (HFM) of the local and regional hydrostratigraphy (Bechtel Nevada, 2002). Hydrostratigraphic units known to exist in the upper approximately 1-km subsurface in the study area are shown on table 1. These units are offset by a series of steeply west-dipping, north-striking normal faults with generally west-side down sense of displacement.

Table 1. Hydrostratigraphic groups
[Modified from Bechtel Nevada (2002)]

Hydrostratigraphic unit	General range in thickness	Comment
Thirsty Canyon volcanic aquifer	60–130 m	Surface outcrops throughout western part of study area west of the West Greeley fault; mainly welded ash-flow tuff and lava.
Timber Mountain volcanic aquifer	150–300 m	Surface outcrops in eastern part of study area, east of the West Greeley fault; underlies Thirsty Canyon volcanic aquifer to west of fault; mainly extra-caldera welded ash-flow tuffs.
Paintbrush volcanic aquifer	30–130 m	Includes a 100-m-thick lava flow east of the West Greeley fault; primarily vitric tuff west of the fault.
Calico Hills volcanic composite unit	100–550 m	Local thickness ranges to as much as 1,300 m; complex three-dimensional distribution of rhyolite lava and zeolitic nonwelded tuff.

The target unit for the magnetotelluric investigation was the Calico Hills VCU. The 12.9 Ma (Sawyer and others, 1994) Calico Hills Formation is a sequence of thick rhyolite lava flows and intercalated variably welded pyroclastic flow deposits and nonwelded pyroclastic fall deposits. These rocks were erupted from vents in two spatially distinct volcanic accumulations – the Calico Hills area (Dickerson and Drake, 1998) and in the vicinity of the buried Area 20 caldera beneath Pahute Mesa. Thick lava flows and intercalated tuffs of the Calico Hills Formation are exposed in the Calico Hills, Fortymile Canyon, and Paintbrush Canyon, and are penetrated in several boreholes at Yucca Mountain (Moyer and Geslin, 1995). Rhyolite lavas within the Calico Hills Formation are only common proximal to source vents (Dickerson and Drake, 1998). More regional studies (Blankennagel and Weir, 1973; pl. 4 of Laczniak and others, 1996) considered the Calico Hills Formation as an aquifer in central and western Pahute Mesa; however, at Well Cluster ER-20-6, lava-flow aquifer composes 50–65 percent of the drill section with the remaining being tuff confining unit. At least three separate lava flows (fractured lava-flow aquifers) were penetrated (Bechtel Nevada, 2002). In northeastern Pahute Mesa and beneath northern Yucca Mountain, relatively minor lava flows are isolated between thick intervals of nonwelded ash-flow tuff (Prothro and Drellack, 1997; Moyer and Geslin, 1995) and the Calico Hills Formation functions as a confining unit (Blankennagel and Weir, 1973; Laczniak and others, 1996), except east of the West Greeley fault, where nonwelded tuffs of the Calico Hills Formation are vitric forming vitric-tuff aquifers. The nonwelded ash-flow tuffs of the Calico Hills Formation are zeolitically altered throughout most of Pahute Mesa, west of the West Greeley fault (Blankennagel and Weir, 1973; Laczniak and others, 1996) and Yucca Flat (Winograd and Thordarson, 1975, IT Corp., 1996).

Electrical Rock Properties

Electromagnetic geophysical methods detect variations in the electrical properties of rock units, in particular, electrical resistivity, in units of ohm-meters [Ωm], or its inverse, electrical conductivity in units of Siemens/meter (S/m). Electrical resistivity can be correlated with geologic units on the surface and at depth using lithologic logs to provide a 3-D picture of subsurface geology. In the upper crust, the resistivities of geologic units are largely dependent upon their fluid content, pore-volume porosity, interconnected fracture porosity, and presence of conductive minerals (for example, clay, graphitic carbon, and metallic). Fluids in the pore spaces and fracture openings, especially saline fluids, can increase electrical conductance in what would otherwise be an electrically resistive rock matrix (Hallenburg, 1998; Hearst and Nelson, 1985; Hearst and others, 2000; Keller, 1987; Keller and Frischknecht, 1966; Palacky, 1987). Although there is not a one-to-one relation between lithology and resistivity, there are general correlations that can be made using typical values, even though values can

be found at other localities (Palacky, 1987) that may fall outside of the ranges presented below. It is common for altered volcanic rocks to contain replacement minerals that have resistivities ten times lower than those of the surrounding rocks (Nelson and Anderson, 1992). Fine-grained sediments, such as clay-rich alluvium, marine shales, and other mudstones, are normally conductive, with resistivities ranging from a few Ωm to tens of Ωm (Keller, 1987; Palacky, 1987). Metamorphic rocks (nongraphitic) and unaltered, unfractured igneous rocks are normally moderately to highly resistive (a few hundred to thousands of Ωm). Carbonate rocks can have similarly high resistivities depending on their fluid content, porosity, and impurities (Keller, 1987; Palacky, 1987). Fault zones may be moderately conductive (tens of Ωm) when composed of rocks fractured enough to have hosted fluid transport and consequent mineralogical alteration (Eberhart-Phillips and others, 1995). At greater depths, higher subsurface temperatures decrease fluid viscosity that causes greater mobility of ions in the fluids and reduces rock resistivity (Hallenburg, 1998). Tables of electrical resistivity for a variety of rocks, minerals, and geological environments may be found in Keller (1989) and Palacky (1987).

Magnetotelluric Method

The magnetotelluric method is a passive ground-based electromagnetic geophysical technique that investigates the distribution of electrical resistivity (or its inverse, electrical conductivity) below the surface at depths of tens of meters to tens of kilometers (Vozoff, 1991). It does so by measuring time variations in the Earth's natural electric and magnetic fields. Worldwide lightning activity at frequencies of about 10,000 hertz to 1 hertz and geomagnetic micropulsations at frequencies of 1 hertz to 0.001 hertz provide the main source of signals used by the magnetotelluric method. The natural electromagnetic waves propagate vertically in the Earth because the very large contrast in the resistivity of the air and the Earth causes a vertical refraction of the electromagnetic wave at the surface (Vozoff, 1972).

The natural electric and magnetic fields are recorded in two orthogonal, horizontal directions (the vertical magnetic field is also recorded). The resulting time-series signals are used to derive tensor apparent resistivities and phases after first converting them to complex cross-spectra using fast Fourier transform (FFT) techniques and least-squares, cross-spectral analysis (Bendat and Piersol, 1971) to solve for a tensor transfer function. If one assumes that the Earth consists of a two-input, two-output, linear system in which the orthogonal magnetic fields are input and the orthogonal electric fields are output, then a transfer function can be calculated that relates the observed electric fields to the magnetic fields. Before it is converted to apparent resistivity and phase, the tensor is normally rotated parallel to geologic strike. Subsurface geologic strike can be estimated by determining the horizontal direction (Hxy or Hyx) that the vertical magnetic field (Hz) "tips" (the Tipper strike direction).

For a two-dimensional (2-D) Earth, the magnetotelluric fields can be decoupled into transverse electric (TE) and transverse magnetic (TM) modes. Two-dimensional resistivity modeling is generally computed to fit both modes. When the geology satisfies the 2-D assumption, the magnetotelluric data for the TE mode is assumed to represent the electric field oriented along geologic strike, and the data for the TM mode is assumed to represent the electric field oriented across strike. The magnetotelluric method is well suited for studying complicated geological environments because the electric and magnetic relations are sensitive to both vertical and horizontal variations in resistivity. High-resolution shallow-subsurface characterization is possible for closely spaced magnetotelluric stations, but the resolution of the subsurface decreases for deeper measurements and for widely spaced stations. The method is capable of establishing whether the electromagnetic fields are responding to subsurface rock bodies of effectively one, two, or three dimensions. An introduction to the magnetotelluric method and

references for a more advanced understanding are contained in Dobrin and Savit (1988) and Vozoff (1991).

Magnetotelluric Data

This survey is essentially a feasibility study for reducing geologic uncertainty in the current framework model for Pahute Mesa. Reducing the uncertainty in the geologic/hydrostratigraphic framework models will also benefit NNSA's strategy for defining good monitoring well locations by having more accurate subsurface characterization of the groundwater barriers.

In October of 2007, the USGS collected 20 magnetotelluric stations at the NTS in Area 20 of Pahute Mesa CAU (numbered 2–24, fig. 1). The station locations were chosen to constrain the geologic and hydrostratigraphic interpretation, for proximity to roads, and to avoid, where possible, electrical noise from power lines and vehicles. The magnetotelluric data were collected with Electromagnetic Instruments, Inc., (EMI) MT-1 system (EMI, 1996). Horizontal electric fields were measured using three copper/copper sulfate porous-pot electrodes placed in an L-shaped array with dipole lengths of 30 meters (m). The orthogonal magnetic fields in the direction of the electric-field measurement array were sensed using EMI's high-magnetic-permeability, mu-metal-cored induction coils. The magnetotelluric data were recorded as non-remote referenced single stations.

Table 2 lists the 20 magnetotelluric station locations as recorded using a GPS during field acquisition. Coordinates are referenced to the 1866 Clarke spheroid and North American 1927 Western United States datum. Longitude and latitude format is degrees, minutes, seconds. Station elevation is given in meters. Universal Transverse Mercator (UTM) Zone 13 Northing and Easting units are in meters. The accuracy of the x, y component is about ±5 m. The accuracy of the z component is about ±10 m. The X direction is given in degrees and defines the direction of the measured magnetic (Hx) and electric (Ex) fields.

Table 2. Magnetotelluric station locations, Area 20, Pahute Mesa, Nevada Test Site, Nevada

Station	North (m)	East (m)	Latitude	Longitude	Elev (m)	Ex (azm)
2	4125846	549944	37:16:46.921	116:26:11.855	1997	330
3	4125594	550793	37:16:38.578	116:25:37.442	1981	340
4	4125689	551689	37:16:41.483	116:25:01.036	1991	41
5	4125603	551944	37:16:38.642	116:24:50.703	2009	320
6	4125451	552372	37:16:33.623	116:24:33.363	2002	195
7	4124749	548996	37:16:11.505	116:26:50.610	1925	96
8	4125042	550123	37:16:20.797	116:26:04.782	1996	152
9	4125051	550708	37:16:20.975	116:25:41.027	1982	206
10	4124815	551192	37:16:13.221	116:25:21.434	1986	230
11	4124798	552070	37:16:12.494	116:24:45.790	2014	200
12	4124914	552263	37:16:16.220	116:24:37.925	2005	194
14	4124007	550059	37:15:47.224	116:26:07.631	1992	175
15	4124440	550769	37:16:01.136	116:25:38.700	1991	138
16	4124281	551362	37:15:55.860	116:25:14.664	1983	128
17	4124423	552032	37:16:00.334	116:24:47.427	2016	234

18	4124274	552458	37:15:55.412	116:24:30.170	2003	18
19	4123467	549744	37:15:29.762	116:26:20.549	1993	125
20	4123561	550118	37:15:32.740	116:26:05.344	1997	204
22	4123639	551153	37:15:35.068	116:25:23.308	1969	24
24	4123569	552463	37:15:32.535	116:24:30.146	2002	55

The recorded time-series data were transformed to the frequency domain and processed to determine the impedance tensor, which is used to derive apparent resistivities and phases at each site. Rotation of the impedance tensor allows for decoupling into the TE and TM modes. The data were all rotated from the original acquisition azimuth, Ex (azm), listed in table 2 above to true north prior to modeling. Cross-power files were sorted to select optimal signal-to-noise time-series datasets (see appendix H).

Three-Dimensional Resistivity Modeling

Drill holes on Pahute Mesa indicate the presence of 3-D structures in the form of lobes of rhyolite lava intercalated within nonwelded tuff (Bechtel Nevada, 2002). One-dimensional or two-dimensional resistivity modeling will produce false conductors if the TE mode data are used in inversions or forward modeling (Wannamaker and others, 1984). Therefore, 3-D resistivity modeling is necessary for this study. Initially, we inverted the magnetotelluric data with Siripunvaraporn's (2005) 3-D inversion program for magnetotelluric data, WSINV3DMT, using a 200 Ωm homogeneous 3-D model space (52x52x24) with 100-m XY cell size in the finer part of the mesh (fig. 2) for the 3-D resistivity inversion starting model. The resulting calculated data misfits to the observed data were poor at the highest frequencies for stations 2–7, 9, 10, 16, 17, and 19 after 5 iterations for the 11 frequencies inverted (0.06 to 86 Hz) requiring 1.0 Gbyte RAM and 4,868 minutes (about 81 hours) on a 2.0 GHz Quad Core Xeon processor using a 64-bit Linux operating system. Consequently, we imported the inversion result into Geosystem's (2007) WinGLink 3-D Forward Modeling module, MT_4, that uses a finite difference algorithm for computing the magnetotelluric response of general 3-D models using the minimum residual relaxation method of Mackie and others (1993; 1994) attempting to fit the higher frequencies of the dataset. The resulting resistivity response is evaluated below and compared with existing well data and hydrogeologic unit tops from the current Pahute Mesa framework model. We interpret nine depth slices and four west-east profile cross sections of the 3-D resistivity inversion model. For each magnetotelluric profile, model depth is relative to the Earth's surface.

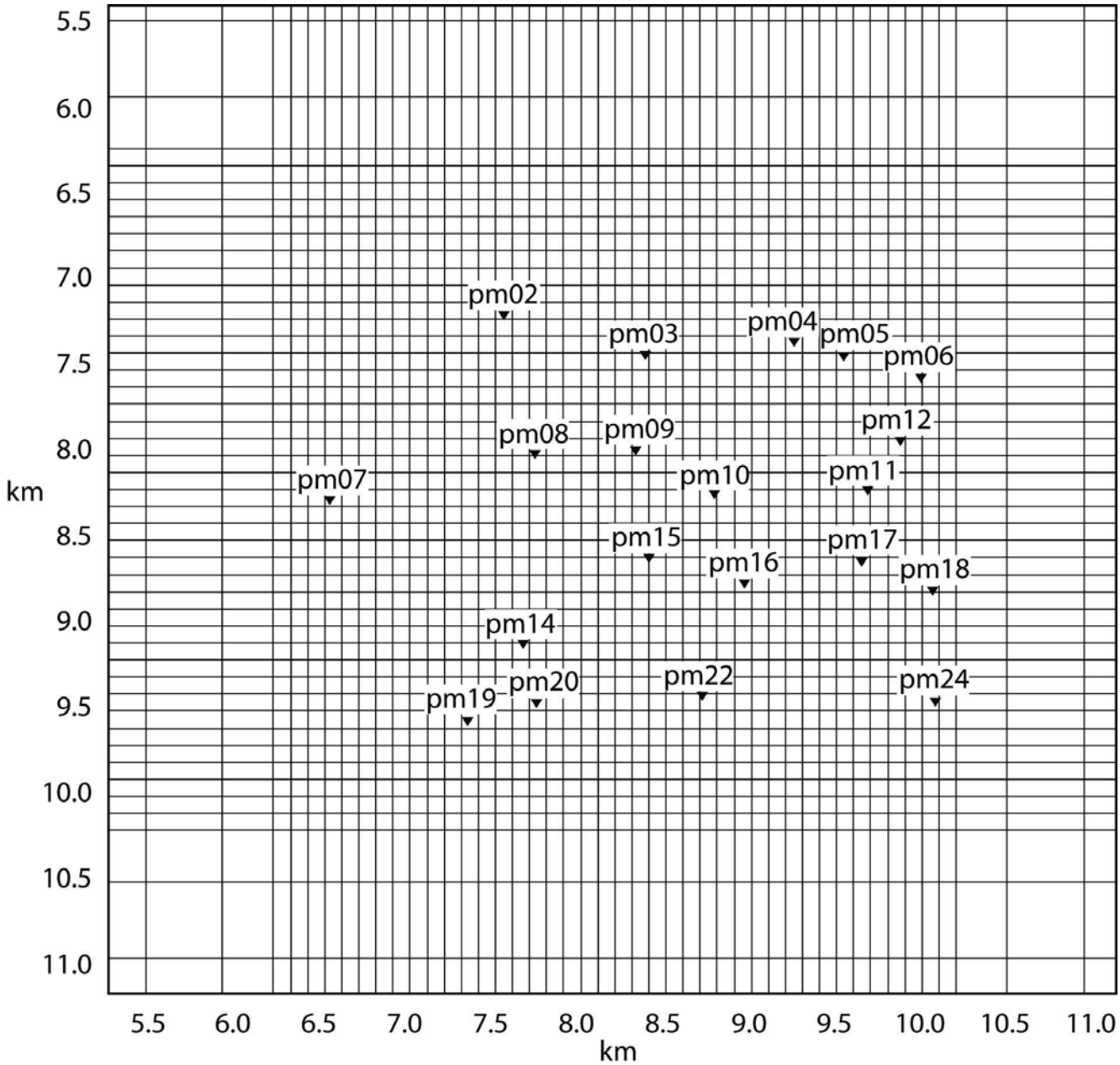

Figure 2. Three-dimensional resistivity model XY mesh, Area 20, Pahute Mesa, Nevada Test Site, Nevada. Black lines are XY mesh boundaries. Black inverted triangles are magnetotelluric stations. Distance scales are kilometers (km) from XY mesh origin.

Discussion

The correlation of resistivity models based on magnetotelluric data with hydrogeologic units is based on well logs and surface geology, mainly rocks cropping out in the vicinity of the magnetotelluric cross section. Where there is little resistivity contrast between adjacent lithologic units, borehole information and a priori knowledge are used to help constrain the models.

The magnetotelluric response from the Calico Hills zeolitic VCU is sensitive to the unit thickness and the resistivity contrast between lava and zeolitic tuff components within the unit. This premise is based on the nearly 4:1 contrast between average resistivities for the Calico Hills zeolitized composite (CHZCM) lava-flow aquifer (LFA) and the CHZCM tuff confining unit (TCU) below the water table (table 3). The magnetotelluric station spacing also affects our ability to resolve resistivity differences within the unit. The larger the magnetotelluric station spacing, the larger the Earth volume averaging during resistivity modeling. This is similar to the thin layer problem in geophysics. The deeper the layer, the thicker it needs to be to be detectable with geophysics (along with sufficient rock property contrast with surrounding host rocks) because a larger volume of Earth is averaged with depth during modeling.

Constraining the geologic interpretation of the 3-D resistivity model begins where we have the most well control with borehole resistivity information in Area 20 of Pahute Mesa, near the well cluster, ER-20-6 (table 3). Three pump test wells (ER20-6#1, ER20-6#2, and ER20-6#3) comprise well cluster ER-20-6 located from 166 to 296 m southwest of the underground (674 m) nuclear test (Bullion) in emplacement hole U-20bd (fig. 1) (Geldon, 2004). Our interpretations begin with resistivity cross-section Profile A, the closest selected east-west resistivity profile to ER-20-6.

Table 3. Hydrostratigraphic and hydrogeologic groups

[Bulk average resistivities in Ωm are from NTS wells PM-1, ER20-5#3, ER20-6#1, ER20-6#2, and ER20-6#3. S, saturated; U, unsaturated; NA, well log data not available]

Hydrogeologic grouping	Abbreviation	Ωm
Alluvial aquifer	AA	NA
Vitric tuff aquifer (vitric tuff units and welded tuff aquifer)	VTA	NA
Welded tuff aquifer (partly to densely welded ash flow tuff)	WTA	NA
Calico Hills zeolitized composite (tuff confining unit)	CHZCM-TCU	71-5906(U)/45-114(S)
Calico Hills zeolitized composite (lava flow aquifer)	CHZCM-LFA	50(U)/161-449(S)
Crater Flat confining unit (tuff confining unit)	CFCU-TCU	36(S)
Bullfrog confining unit (tuff confining unit)	BFCU-TCU	42(S)
Belted Range aquifer (lava flow aquifer)	BRA-LFA	81(S)
Belted Range aquifer (welded tuff aquifer)	BRA-WTA	76(S)
Belted Range aquifer (confining unit)	BRA-TCU	71(S)
Pre-Belted Range composite	PBRCM	NA

Appendixes A, B, and C contain depth slices and cross sections of the 3-D resistivity forward model without geologic interpretations. Appendix D contains plots showing the observed and calculated apparent resistivity and phase curves of the forward 3-D model. Appendixes E, F, and G contain depth

slices and cross sections of the 3-D resistivity inversion model without geologic interpretations. Appendix H contains plots showing the observed and calculated apparent resistivity and phase curves of the inverted 3-D model. Appendix I contains the following magnetotelluric parameter plots for each station: Apparent resistivity, impedance phase, rotation angle, impedance skew, multiple coherency, impedance polar plots, tipper magnitude, tipper strike, and HzHx and HzHy coherency.

Profile A (Stations 19–24)

The resistivity model along this profile (fig. 3) reveals generally resistive (greater than 100 Ωm) rocks above the water table at approximately 616–618 m depth (Geldon, 2004) and generally conductive (less than 100 Ωm) rocks below the water table on top of generally resistive (greater than 100 Ωm) rocks at depths greater than about 1,200 m. Exceptions to this pattern are shallower conductive rocks east of an unnamed fault east of magnetotelluric station 24 and more resistive rocks just below the water table near the nuclear emplacement wells U-20b, U-20bd#1, and U-20ap. The shallower conductive rocks east of station 24 are interpreted to be a shallower horizon of conductive CHZCM on top of conductive CFCU and BFCU (table 3). The resistive rocks just below the water table near emplacement wells U-20b and U-20bd#1 may be an indicator of increased permeability from zones of intense deformation. The resistive rocks just below the water table near emplacement well U-20ap may also be an indicator of increased permeability, but also may be from lesser amounts of zeolitized tuffs in the Calico Hills vitric composite (CHVCM) found in this well near the water table, although its true thickness is unknown.

Resistive rocks above the water table correspond to rocks of Thirsty Canyon volcanic aquifer (TCVA), Timber Mountain aquifer (TMA), and Paintbrush vitric tuff aquifer (PVTA) seen in wells U-20b, ER-20-6, U-20ap, and in nearby surface outcrops of TCVA west of the West Greeley fault and TMA east of the West Greeley fault.

The 3-D resistivity inversion did not resolve the individual TCU and LFA units within the CHZCM that occurs at about 600-m depth near ER-20-6. Instead, CHZCM correlates with a 75 Ωm zone beneath station 22 (fig. 3) and a 150 Ωm zone beneath projections of wells ER-20-6 and U-20bd#1. CHZCM-LFA in these wells vary in thickness from about 30 to 185 m, whereas CHZCM-TCU varies in thickness from about 10 to 245 m. The inversion's failure to resolve even the thickest occurrence of TCU and LFA in ER-20-6 may be due to the large magnetotelluric station spacing between stations 22 and 24 that forced the inversion to average larger than anticipated rock volumes at about 600- to 1,000-m depth between stations that were 1,300 m apart. Originally, magnetotelluric stations were planned to be 600 m apart, but site logistics prevented collecting a magnetotelluric station (the "missing" station 23) between stations 22 and 24. The original premise was that magnetotelluric station spacing of about 600 m would be able to resolve individual layers of TCU and LFA, presuming about a 4:1 resistivity contrast between TCU and LFA (table 3).

The generally resistive (greater than 100 Ωm) rocks at depths greater than about 1,200 m beneath the profile are not well constrained as the magnetotelluric response is a general increase in resistivity (fig. 3). The depths of inferred BFCU and BRA, and inferred pre-Belted Range composite (PBRCM) are based on projected boundaries from deep well PM-1 (fig. 6) in the northeast corner of the survey area and may be deeper or shallower than shown (fig. 3). The inferred fault offset on the hanging wall side of the Boxcar fault is not well constrained, but was guided by the generally deepening 75 Ωm conductor west of station 19.

The inferred west-dipping fold in interpreted layers west of Buteo fault is not required by the magnetotelluric data along this profile, but was guided by the interpreted cross section appearing on plate 4 of Laczniak and others (1996).

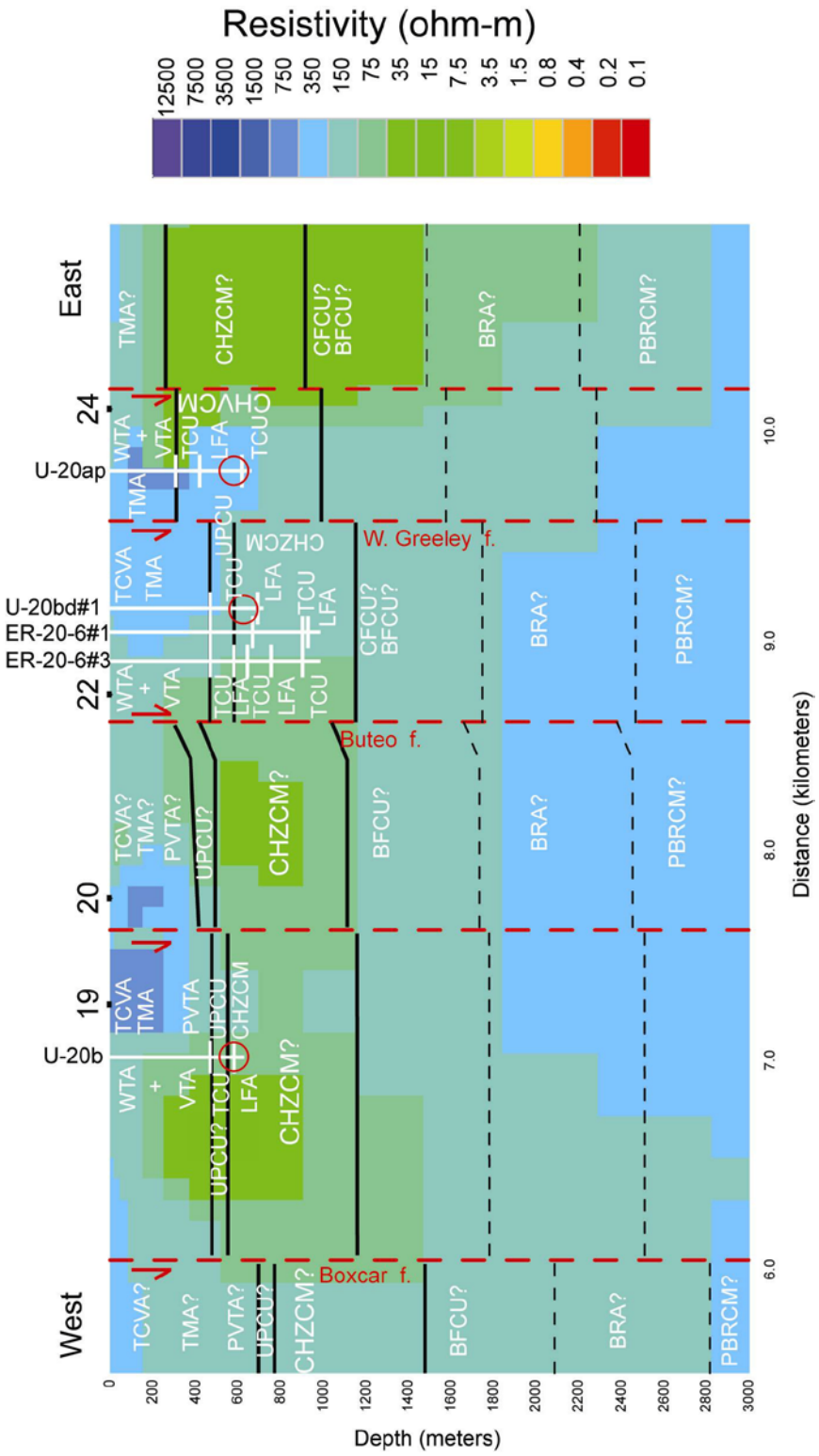

Figure 3. Profile A (fig. 1) resistivity model cross section with hydrogeologic interpretation. Refer to table 3 for key to hydrogeologic units. White lines are projected well horizons. Black numbers at surface are magnetotelluric stations. Black lines are interpreted hydrogeologic boundaries. Red dashed lines are projected faults.

Profile B (Stations 13–18)

The resistivity model along this profile (fig. 4) also reveals generally resistive (greater than 100 Ω–m) rocks above the water table at about 600-m depth and generally conductive (less than 100 Ωm) rocks below the water table on top of generally resistive (greater than 100 Ωm) rocks at depths greater than about 1,000 m. Exceptions to this pattern are shallower conductive (35–75 Ωm) rocks beneath magnetotelluric station 15 and more resistive (greater than 100 Ωm) rocks just below the water table near nuclear emplacement wells U-20ai and U-20am, and also below magnetotelluric stations 16 and 17. The shallower conductive rocks beneath magnetotelluric station 15 are interpreted to be a shallower horizon of conductive CHZCM. The resistive rocks just below the water table near wells U-20ai and U-20am may be an indicator of increased permeability from zones of intense deformation. Alternatively, the resistive rocks near well U-20am may be from lesser amounts of zeolitized tuffs in the Calico Hills vitric composite (CHVCM) found in this well near the water table.

Resistive rocks above the water table generally correspond to TCVA, TMA, and PVTA seen in wells U-20ai and U-20am, and in nearby surface outcrops of TCVA west of the West Greeley fault and TMA east of the West Greeley fault. Resistive rocks near the water table below magnetotelluric stations 16 and 17 are inferred to be CHVCM as seen in well U-20am, although its true thickness is unknown.

The generally resistive (greater than 100 Ωm) rocks at depths greater than about 1,000 m beneath the profile are not well constrained as the magnetotelluric response is a general increase in resistivity. The depths of inferred BFCU and BRA, and inferred PBRCM are based on projected boundaries from deep well PM-1 (fig. 6) and may be deeper or shallower than shown (fig. 4).

There is also a general increase in resistivity beneath the Buteo fault from about 400-m to about 1,800-m depth compared with the resistivity variations west and east of the fault, and also compared to the same fault on resistivity Profile A to the south (fig. 3). This may be related to an increase in permeability near this fault.

The inferred west-dipping fold in interpreted layers west of Buteo fault may not be required by the magnetotelluric data along this profile, but was guided by the west-dipping conductor beneath station 15.

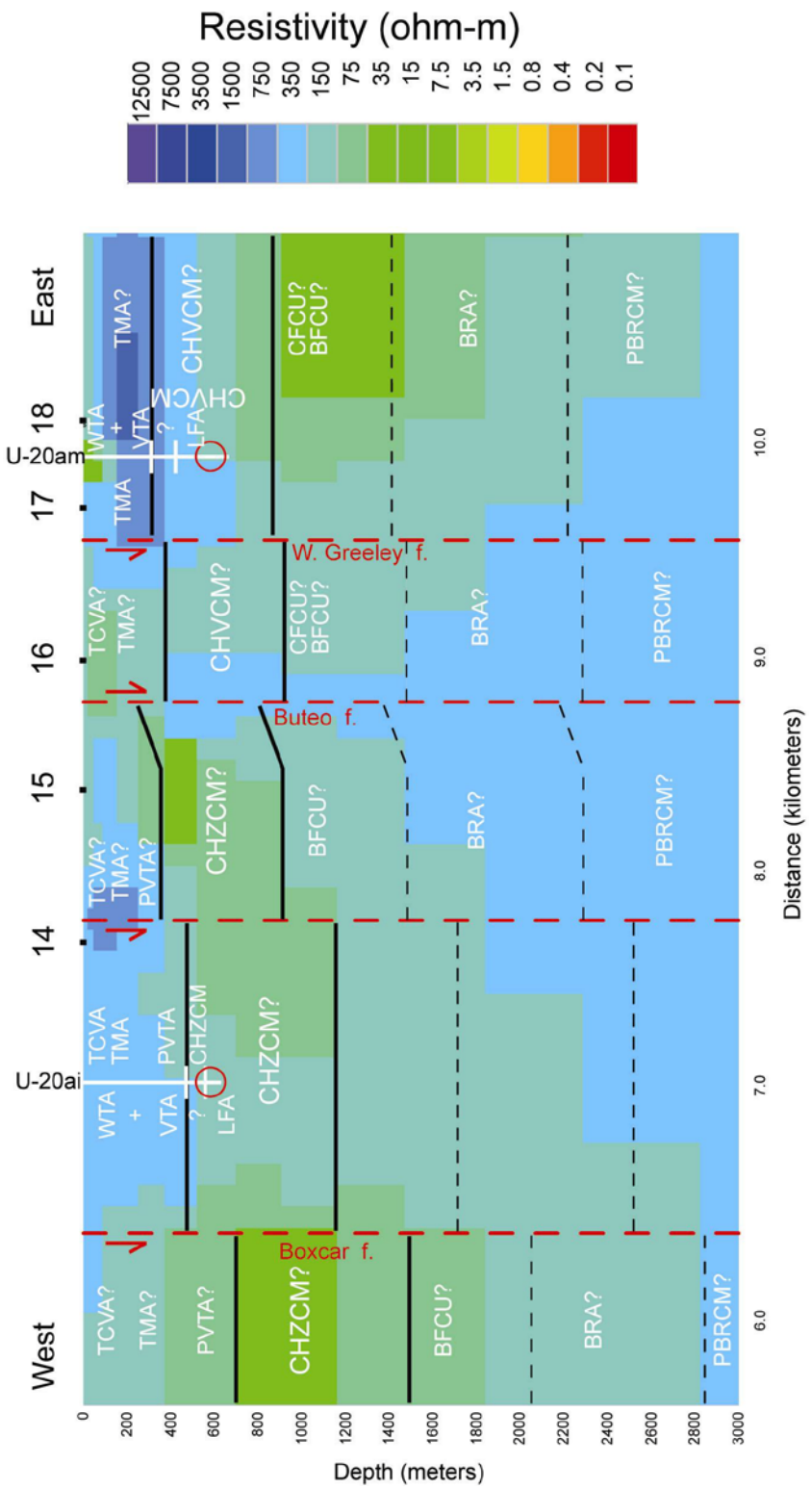

Figure 4. Profile B (fig. 1) resistivity model cross section with hydrogeologic interpretation. Refer to table 3 for key to hydrogeologic units. White lines are projected well horizons. Black numbers at surface are magnetotelluric stations. Black lines are interpreted hydrogeologic boundaries. Red dashed lines are projected faults.

Profile C (Stations 7–12)

The resistivity model along this profile (fig. 5) reveals similar resistive and conductive patterns as Profiles A (fig. 3) and B (fig. 4) with the greatest exception being even more resistive (greater than 300 Ωm) rocks in the center of the profile below magnetotelluric stations 8 and 9. The resistive rocks below these stations may be an indicator of an even larger volume of increased permeability.

Resistive rocks above the water table generally correspond to TCVA, TMA, and PVTA seen in wells UE-20h and U-20ab, and in nearby surface outcrops of TCVA west of the West Greeley fault and TMA east of the West Greeley fault.

Conductive (15–75 Ωm) rocks near the water table adjacent to and east of resistive (150–1500 Ωm) CHVCM seen in well U-20ab are interpreted to be CHZCM on top of CFCU and BFCU. Conductive (75 Ωm) rocks just above the water table east of magnetotelluric station 10 are interpreted to be CHZCM.

The inferred depths of CHZCM (fig. 5) are primarily guided by projected depths from wells UE-20h and U-20ab. The depths of inferred BFCU and BRA, and inferred PBRCM are based on projected boundaries from deep well PM-1 (fig. 6) and may be deeper or shallower than shown (fig. 5).

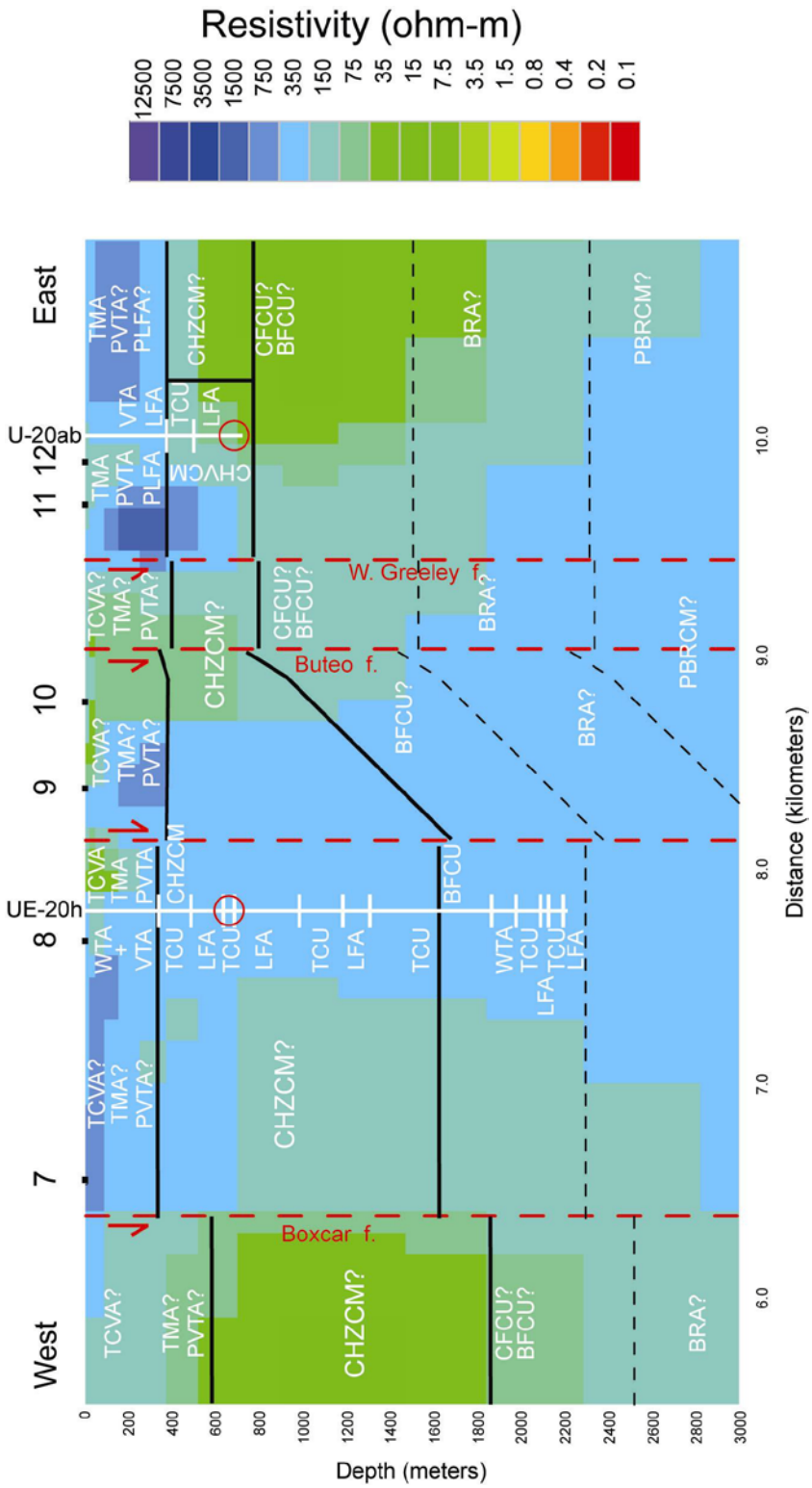

Figure 5. Profile C (fig. 1) resistivity model cross section with hydrogeologic interpretation. Refer to table 3 for key to hydrogeologic units. White lines are projected well horizons. Black numbers at surface are magnetotelluric stations. Black lines are interpreted hydrogeologic boundaries. Red dashed lines are projected faults.

Profile D (Stations 2–6)

The resistivity model along this profile (fig. 6) reveals similar resistive and conductive patterns as Profile C (fig. 5) with the greatest exception being more conductive (less than 100 Ωm) rocks in the upper 2 km between the Buteo and West Greeley faults (fig. 6). These conductive rocks may be an indicator of an area of decreased permeability. Another difference is inferred CHZCM appears to thin and become shallow west of the unnamed fault between the Boxcar and Buteo faults, whereas on Profile C, CHZCM does not thin until east of the unnamed fault (fig. 5).

Resistive rocks above the water table generally correspond to TCVA, TMA, and PVTA seen in wells U-20af, U-20aw, and PM-1, and in nearby surface outcrops of TCVA west of the West Greeley fault and TMA east of the West Greeley fault.

The inferred boundaries of CHZCM (fig. 6) are primarily guided by the similar resistivity pattern seen along Profile C and the projected boundary from well UE-20h (fig. 5), and from wells U-20aw and PM-1 (fig. 6). The boundaries of inferred BFCU and BRA, and inferred pre-Belted Range composite (PBRCM), are based on projections from PM-1 and may be deeper or shallower than shown (fig. 6).

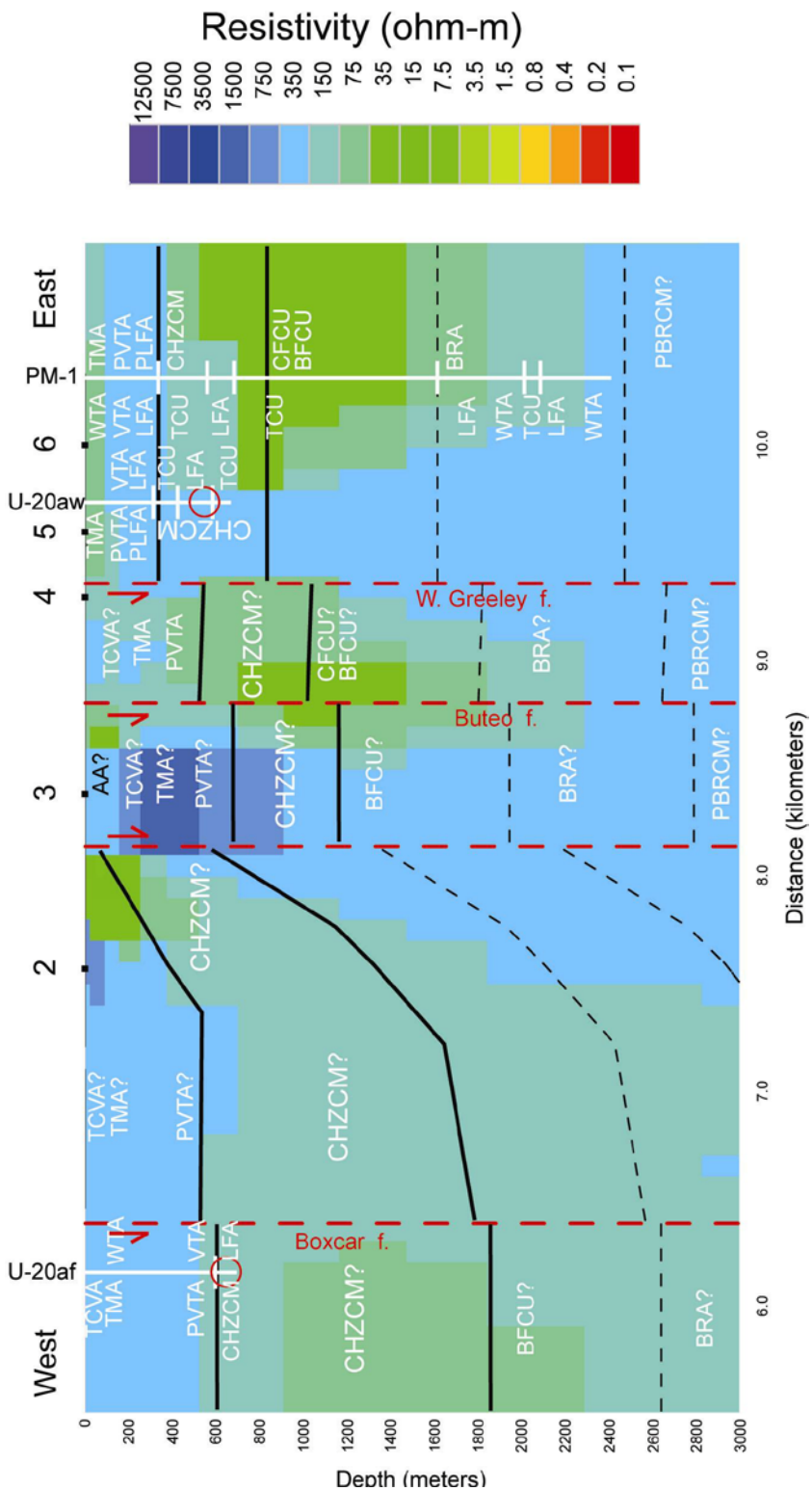

Figure 6. Profile D (fig. 1) resistivity model cross section with hydrogeologic interpretation. Refer to table 3 for key to hydrogeologic units. White lines are projected well horizons. Black numbers at surface are magnetotelluric stations. Black lines are interpreted hydrogeologic boundaries. Red dashed lines are projected faults.

Depth Slices

Appendix A contains all depth slices of the 3-D resistivity forward model without geologic interpretations. We interpret depth slices from just above the water table (about 600 m) to a depth interpreted to be below BFCU (from 525-m to 2.8-km depth).

At 525-m depth (fig. 7), the 3-D resistivity model shows a large portion of the study area to be conductive, which we interpret to be mainly composed of CHZCM. Exceptions are a resistive pattern in the eastern portion of the area we interpret to be CHVCM that appears to be partially bounded by the West Greeley fault and an unnamed fault east of magnetotelluric station 24 (pm24 in fig. 7) and a resistive block encompassing magnetotelluric station 3 (pm03) that we interpret to be PVTA. Another resistive pattern that is consistent from this depth slice to the 1.5-km-depth slice (fig. 11) is in the northern portion of the study area. We interpret this increase in resistivity to be related to an increase in permeability, suggesting that the southern portion of the study area may be less permeable near the southern margin of the Silent Canyon caldera complex (Geldon, 2004). An exception to the northern resistive pattern is more conductive rocks near magnetotelluric station 2 (pm02) and north of the area between magnetotelluric stations 3 (pm03) and 5 (pm05). These geologic interpretations are constrained by wells U-20b, ER-20-6#1, ER-20-6#2, ER-20-6#3, U-20bd#1, U-20ap, U-20ai, U-20am, UE-20h, U-20ab, U-20af, U-20aw, and PM-1 that penetrate this horizon.

At 705-m depth (fig. 8), the 3-D resistivity model shows an even larger portion of the study area to be conductive that we also interpret to be mainly composed of CHZCM. The northern head of the resistive area we interpret to be CHVCM in the depth slice above (fig. 7) appears to be replaced by shallower horizons of BFCU based on depth projections from well PM-1 (fig. 5). The more resistive CHVCM also appears to be partially bounded by the unnamed fault east of magnetotelluric station 24 where more conductive rocks we interpret to be CHZCM appear east of the fault (fig. 8). Again, the northern resistive pattern seen in the depth slice above (fig. 7) is also seen in this depth slice (fig. 8) suggesting that this increase in resistivity may be related to an increase in permeability. The conductive-rock exception in the northern area seen in the depth slice above (fig. 7) continues in this depth slice (fig. 8) near magnetotelluric stations 2 and between stations 3 and 5. These geologic interpretations are constrained by wells ER-20-6#1, ER-20-6#2, ER-20-6#3, U-20bd#1, UE-20h, U-20ab, and PM-1 that penetrate this horizon, and also by minor extensions of wells U-20b, U-20ap, U-20ai, U-20am, U-20af, and U-20aw that nearly penetrate this horizon.

At 915-m depth (fig. 9), the 3-D resistivity model is very similar to the depth slice above (fig. 8), except certain horizons of inferred CHZCM and CHVCM in the eastern portion of the survey area appear to be replaced by interpreted horizons of BFCU based on depth projections from well PM-1 (figs. 3-6). Again, the northern resistive pattern seen in the depth slices above (figs. 7 and 8) is also seen in this depth slice (fig. 9) suggesting that this increase in resistivity may be related to an increase in permeability. The conductive rock exception in the northern area seen in the depth slices above continues in this depth slice near magnetotelluric station 2 and between stations 3 and 5. These geologic interpretations are constrained only by wells ER-20-6#1, ER-20-6#2, ER-20-6#3, UE-20h, and PM-1 that penetrate this horizon, and so have less certainty than the depth slices above (figs. 7 and 8).

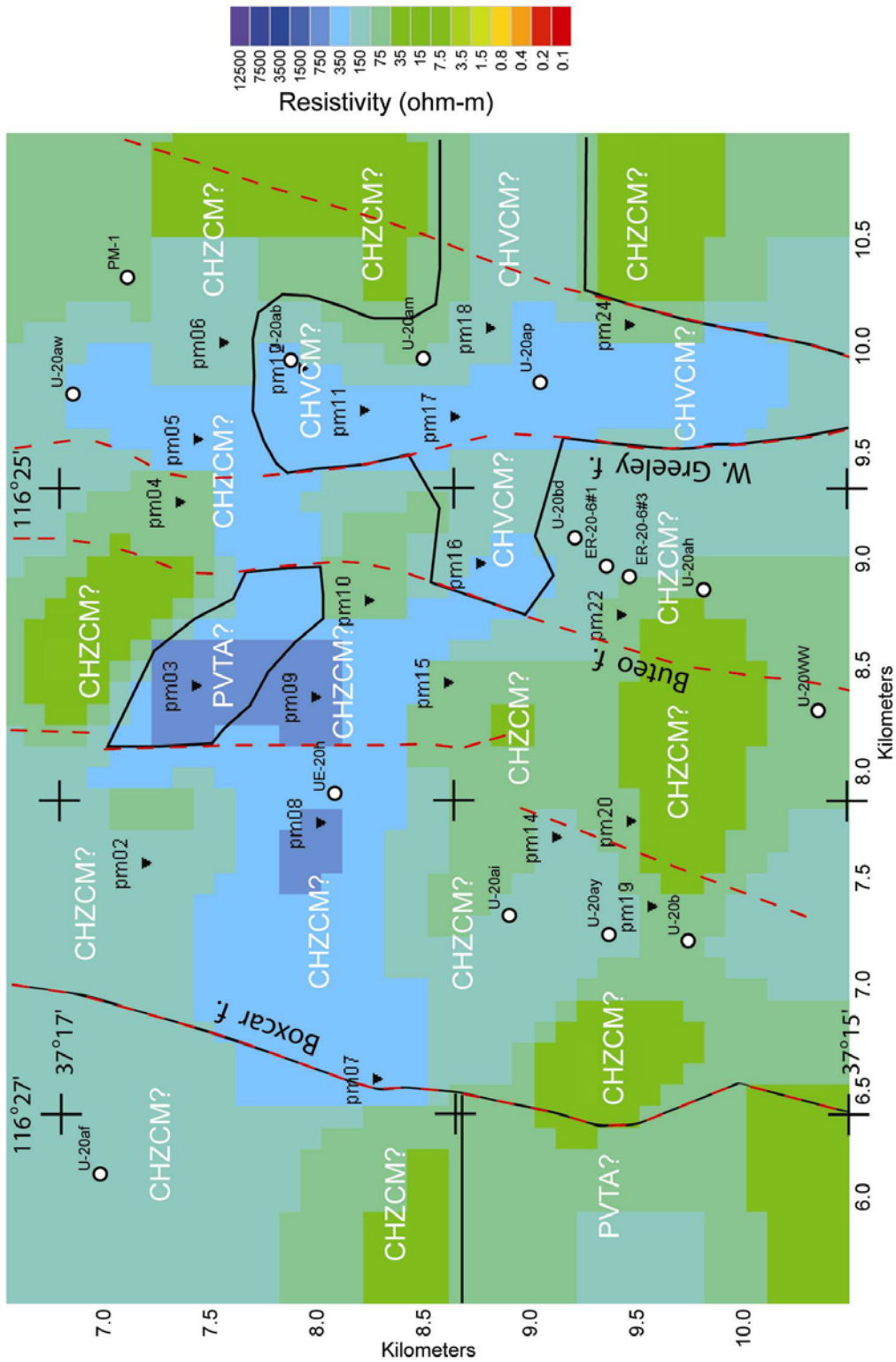

Figure 7. Three-dimensional resistivity model 525-m-depth slice. Refer to table 3 for key to hydrogeologic units. White circles are nuclear drill holes or wells. Black inverted triangles are magnetotelluric stations. Black lines are interpreted hydrogeologic boundaries. Red dashed lines are projected faults.

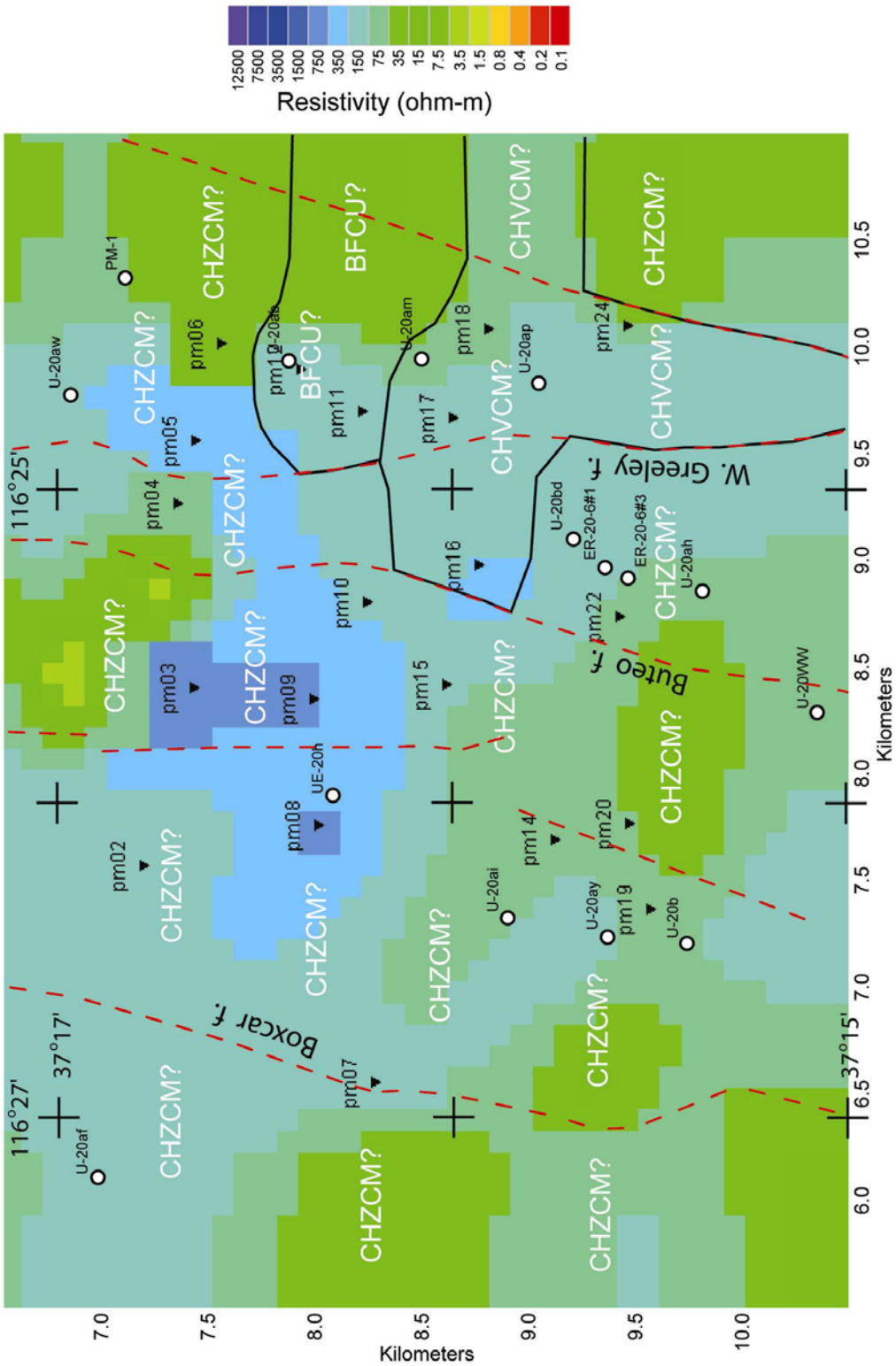

Figure 8. Three-dimensional resistivity model 705-m-depth slice. Refer to table 3 for key to hydrogeologic units. White circles are nuclear drill holes or wells. Black inverted triangles are magnetotelluric stations. Black lines are interpreted hydrogeologic boundaries. Red dashed lines are projected faults.

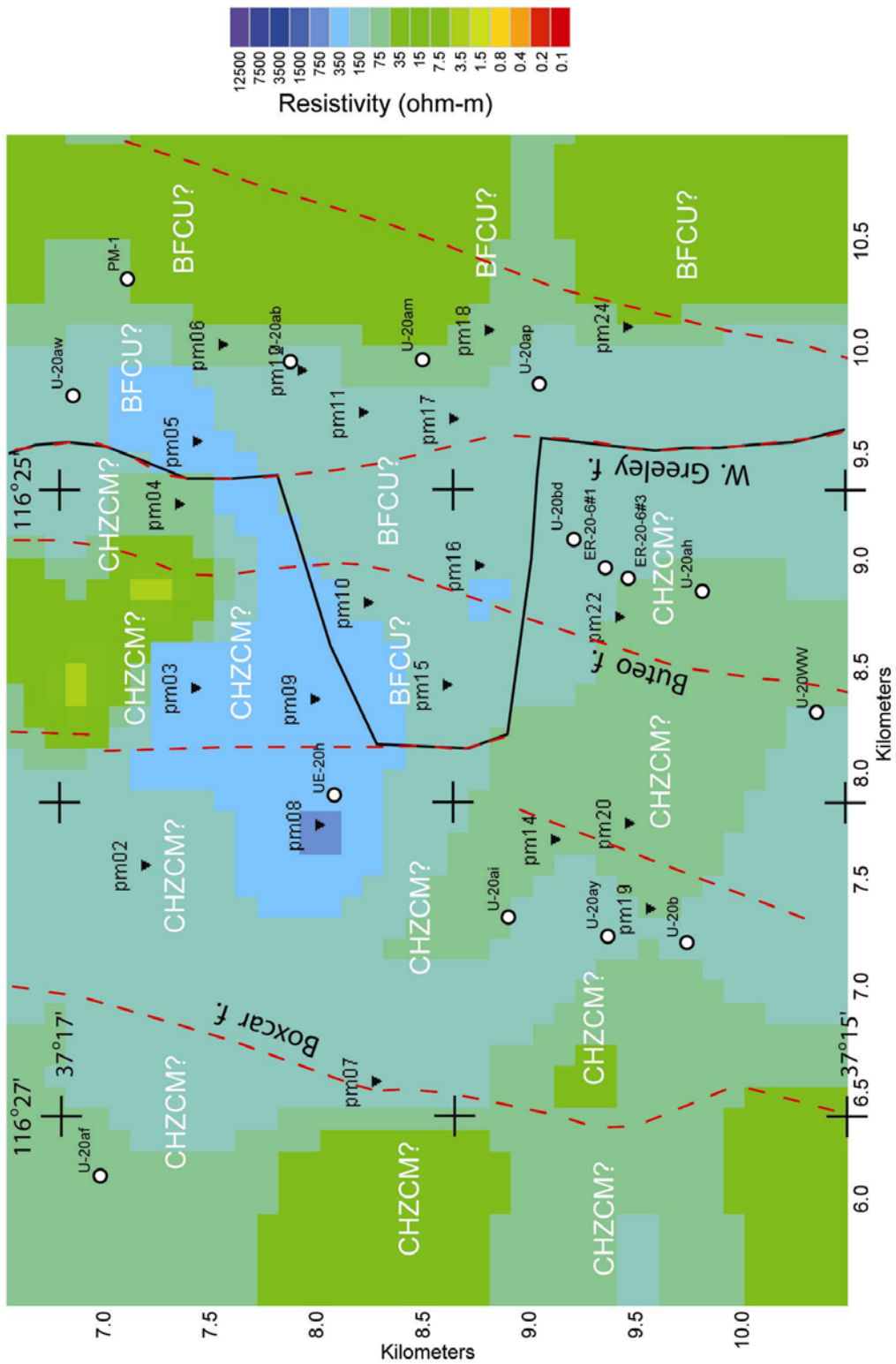

Figure 9. Three-dimensional resistivity model 915-m-depth slice. Refer to table 3 for key to hydrogeologic units. White circles are nuclear drill holes or wells. Black inverted triangles are magnetotelluric stations. Black lines are interpreted hydrogeologic boundaries. Red dashed lines are projected faults.

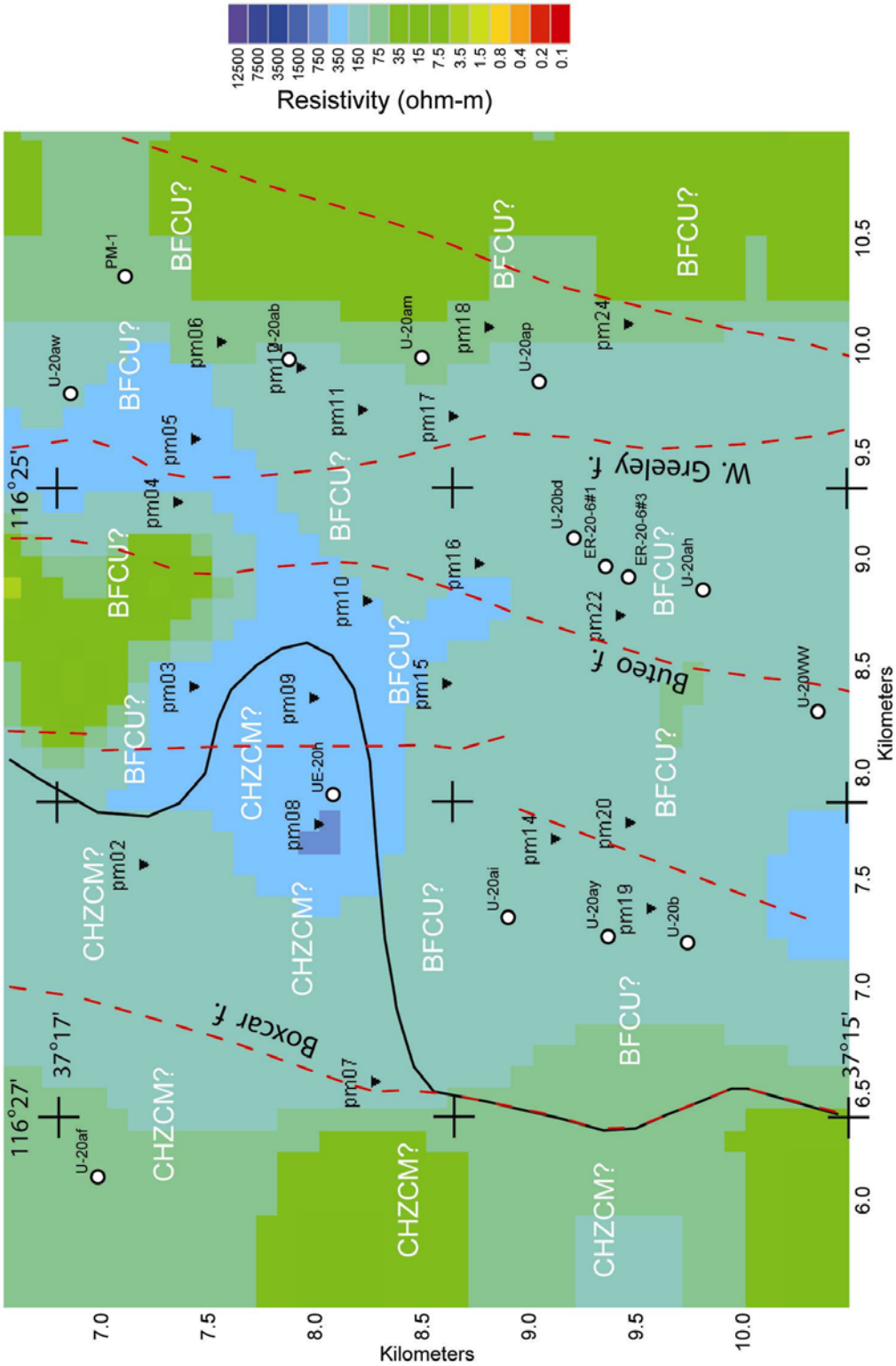

Figure 10. Three-dimensional resistivity model 1.2-km-depth slice. Refer to table 3 for key to hydrogeologic units. White circles are nuclear drill holes or wells. Black inverted triangles are magnetotelluric stations. Black lines are interpreted hydrogeologic boundaries. Red dashed lines are projected faults.

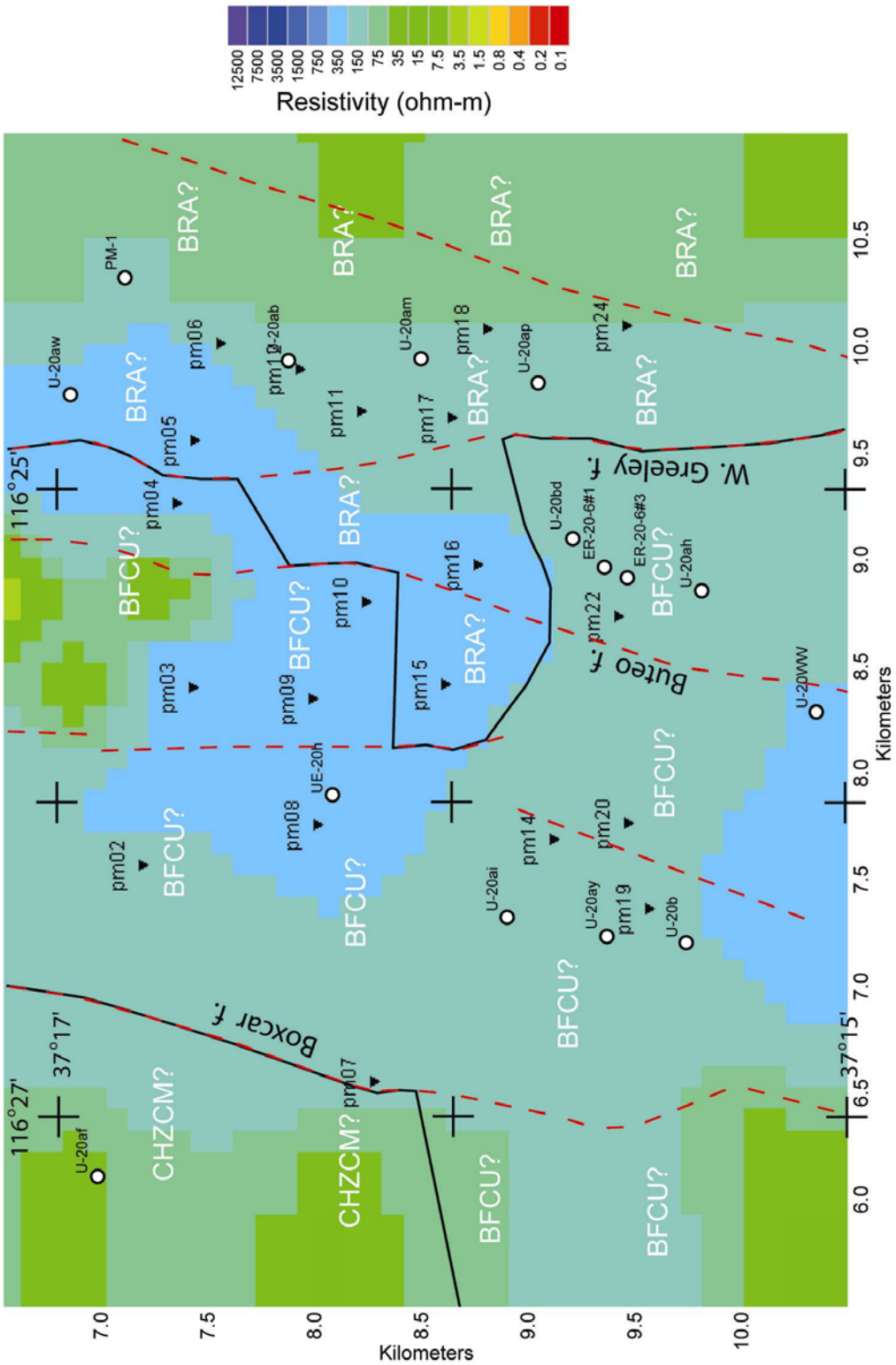

Figure 11. Three-dimensional resistivity model 1.5-km-depth slice. Refer to table 3 for key to hydrogeologic units. White circles are nuclear drill holes or wells. Black inverted triangles are magnetotelluric stations. Black lines are interpreted hydrogeologic boundaries. Red dashed lines are projected faults.

At 1.2-km depth (fig. 10), the 3-D resistivity model is similar to the depth slice above (fig. 9), though slightly more resistive overall with inferred horizons of CHZCM in the central portion of the survey area replaced by interpreted horizons of BFCU based on depth projections from well PM-1. Again, the northern resistive pattern seen in the depth slices above (figs. 7-9) is also seen in this depth slice (fig. 10) suggesting that this increase in resistivity may be related to an increase in permeability. The conductive rock exception in the northern area seen in the depth slices above continues in this depth slice near magnetotelluric station 2 and between stations 3 and 5. These geologic interpretations are constrained only by wells UE-20h and PM-1 that penetrate this horizon, and so have even less certainty than the depth slice above (fig. 9).

At 1.5-km depth (fig. 11), the 3-D resistivity model is similar to the depth slice above (fig. 10), though slightly more resistive overall with inferred horizons of CHZCM in the western portion of the survey area replaced by horizons of BFCU and inferred horizons of BFCU in the eastern portion of the survey area replaced by interpreted horizons of BRA, each based on depth projections from well PM-1. Again, the northern resistive pattern seen in the depth slices above (figs. 7-10) is also seen in this depth slice (fig. 11) suggesting that this increase in resistivity may be related to an increase in permeability. The conductive rock exception in the northern area seen in the depth slices above continues in this depth slice near magnetotelluric station 2 and between stations 3 and 5. These geologic interpretations are also constrained only by wells UE-20h and PM-1 that penetrate this horizon, and so have less certainty over much of the survey area.

At 1.9-km depth (fig. 12), the 3-D resistivity model is somewhat similar to the depth slice above (fig. 11), primarily in the western portion of the survey area, whereas the central and eastern portion of the survey area is more resistive (fig. 12). All inferred horizons of CHZCM in the western portion of the survey area in the depth slice above (fig. 11) are replaced by interpreted horizons of BFCU (fig. 12) and much of the inferred horizons of BFCU in the central portion of the survey area (fig. 11) are replaced by interpreted horizons of BRA (fig. 12), each based on depth projections from well PM-1. These geologic interpretations are constrained only by wells UE-20h and PM-1 that penetrate this horizon, and so have less certainty over much of the survey area.

At 2.3-km depth (fig. 13), the 3-D resistivity model is very similar to the depth slice above (fig. 12), though slightly more resistive overall (fig. 13). All inferred horizons of BFCU in the western portion of the survey area in the depth slice above (fig. 12) are replaced by interpreted horizons of BRA (fig. 13) except in the far northwestern corner of the survey area, and much of the inferred horizons of BRA in the central and eastern portion of the survey area (fig. 12) are replaced by interpreted horizons of PBRCM (fig. 13); each is based on depth projections from well PM-1. These geologic interpretations are constrained only by well PM-1 that penetrates this horizon, and also by a minor extension of well UE-20h, and so have less certainty over much of the survey area.

At 2.8-km depth (fig. 14), the 3-D resistivity model is more resistive than the depth slice above (fig. 13), except in the northwestern and far southwestern corners of the survey area (fig. 14). Inferred horizons of BRA are now restricted to the northwestern portion of the survey area with interpreted horizons of PBRCM occupying the rest of the survey area. These geologic interpretations are not constrained by any wells that penetrate this horizon, so have the largest uncertainty of any of the depth slices.

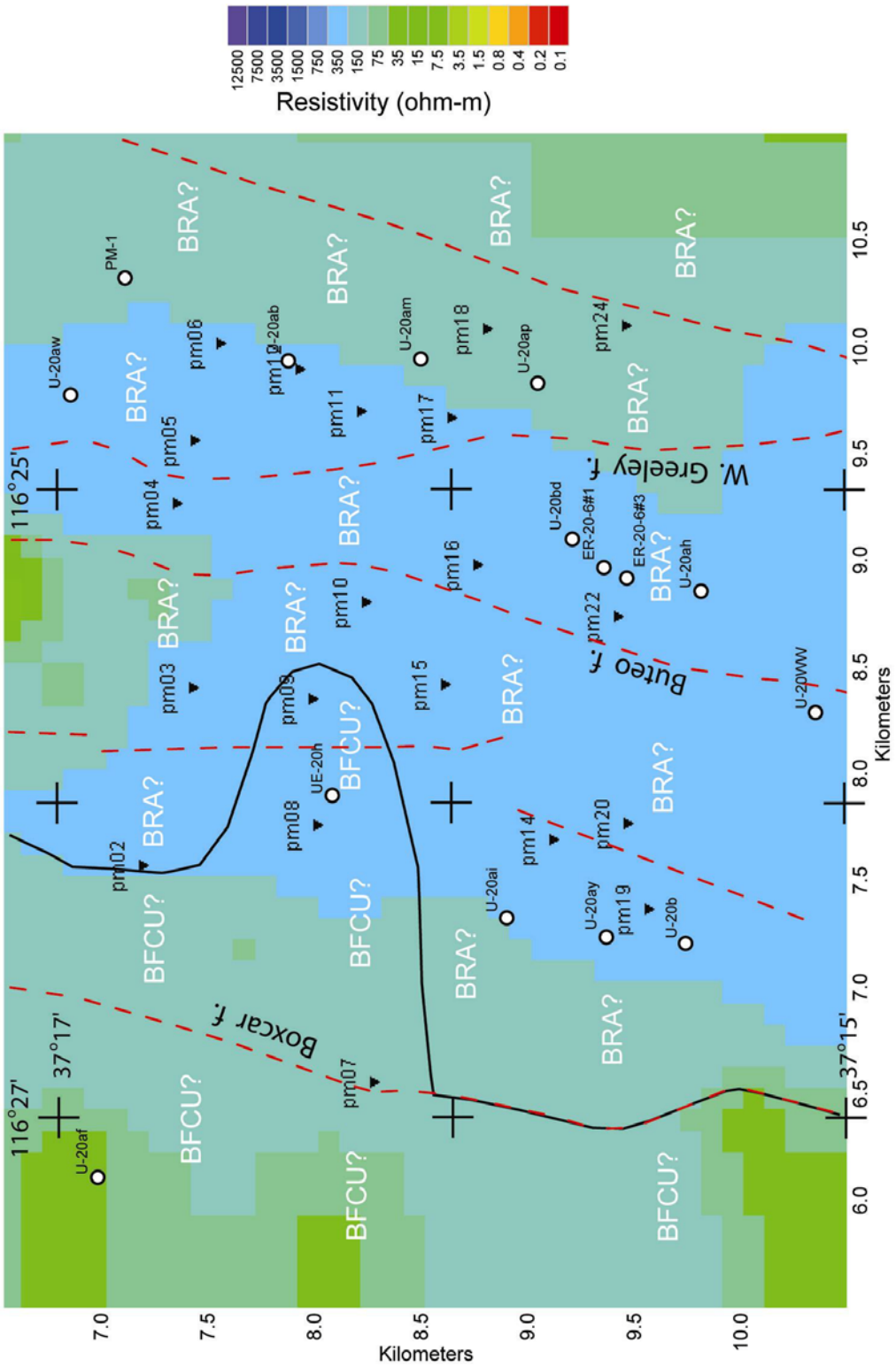

Figure 12. Three-dimensional resistivity model 1.9-km-depth slice. Refer to table 3 for key to hydrogeologic units. White circles are nuclear drill holes or wells. Black inverted triangles are magnetotelluric stations. Black lines are interpreted hydrogeologic boundaries. Red dashed lines are projected faults.

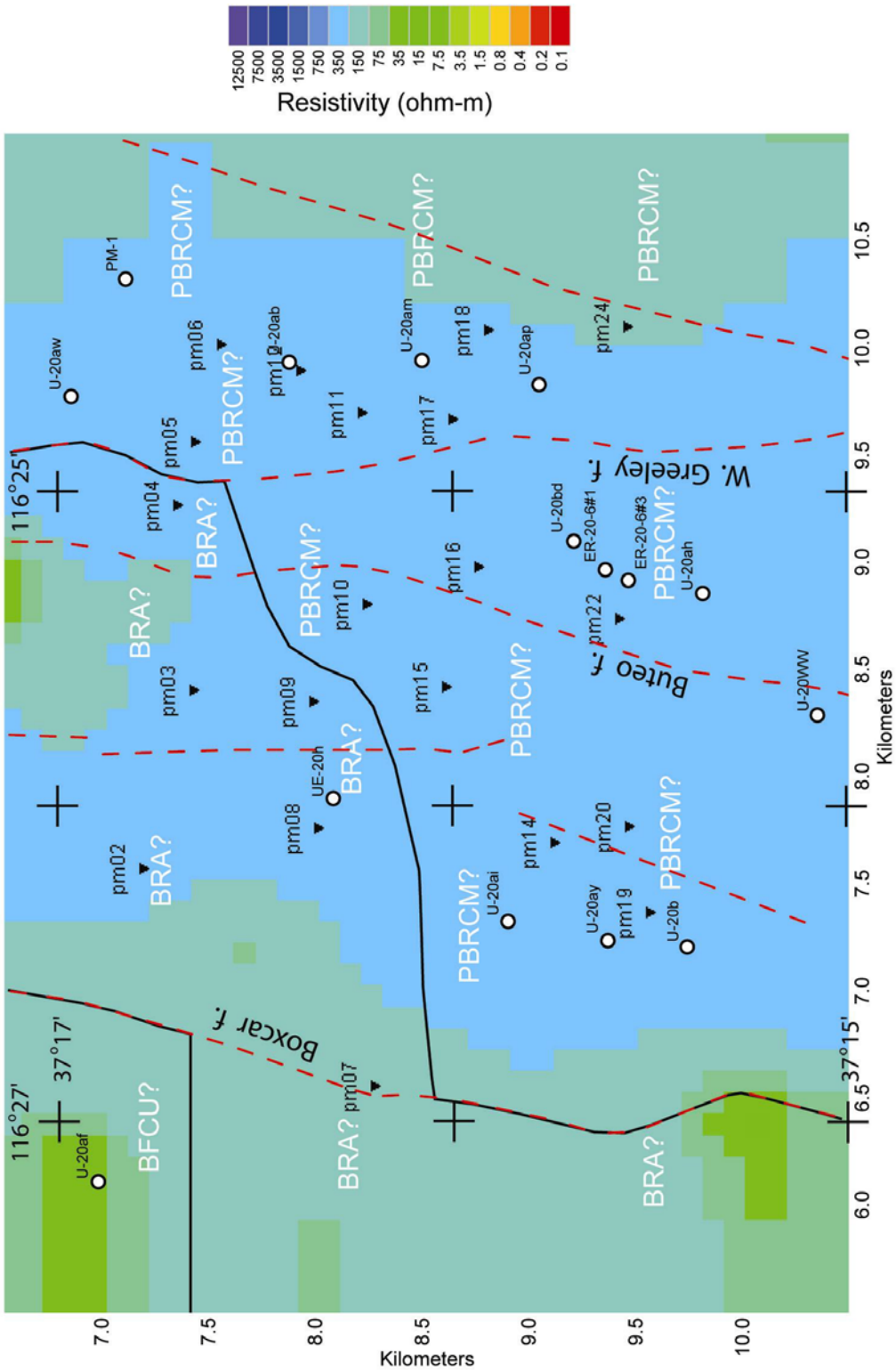

Figure 13. Three-dimensional resistivity model 2.3-km-depth slice. Refer to table 3 for key to hydrogeologic units. White circles are nuclear drill holes or wells. Black inverted triangles are magnetotelluric stations. Black lines are interpreted hydrogeologic boundaries. Red dashed lines are projected faults.

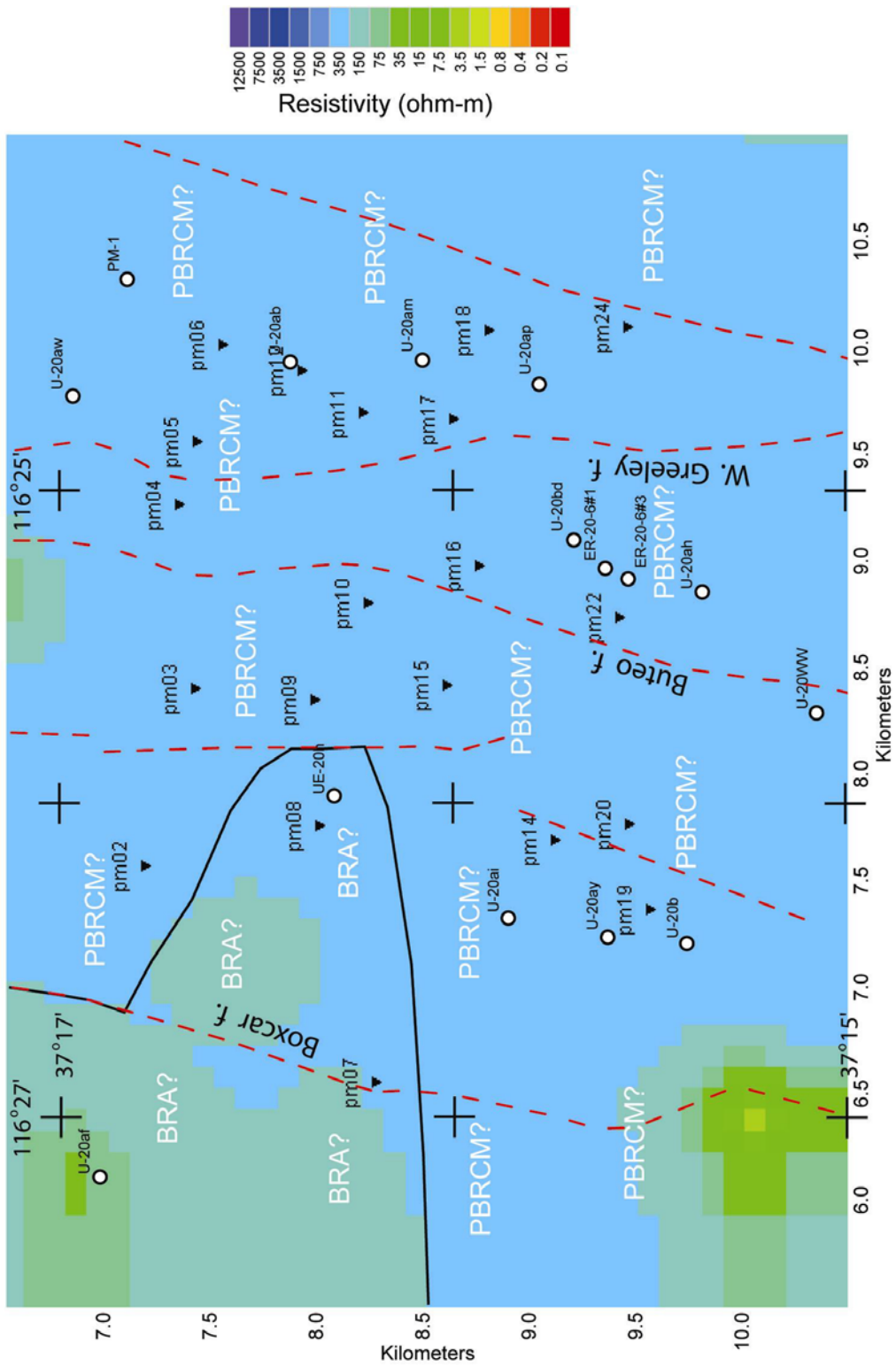

Figure 14. Three-dimensional resistivity model 2.8-km-depth slice. Refer to table 3 for key to hydrogeologic units. White circles are nuclear drill holes or wells. Black inverted triangles are magnetotelluric stations. Black lines are interpreted hydrogeologic boundaries. Red dashed lines are projected faults.

Summary

The three-dimensional resistivity model presented reflects the diffusive nature of the magnetotelluric fields and is a bulk-average representation of the subsurface geology. The resistivity model misfits with well data near well cluster ER-20-6 reveal that the nominal 600-m magnetotelluric station spacing was too coarse to resolve continuity of the tuff confining units between stations.

The resistivity model reveals generally resistive (greater than 100 Ωm) rocks above the water table (about 600-m depth) and generally conductive (less than 100 Ωm) rocks below the water table on top of generally resistive (greater than 100 Ωm) rocks at depths greater than about 1,000 m. Exceptions to this pattern are more resistive rocks just below the water table near the nuclear emplacement wells U-20b, U-20bd#1, and U-20ai. The resistive rocks just below the water table near these emplacement wells may be an indicator of increased permeability from zones of intense deformation. Resistive rocks above the water table correspond to rocks of Thirsty Canyon volcanic aquifer, Timber Mountain aquifer, and Paintbrush vitric tuff aquifer seen in nearby wells and in nearby surface outcrops of Thirsty Canyon volcanic aquifer west of the West Greeley fault and Timber Mountain aquifer east of the West Greeley fault.

A resistive pattern that is consistent from 525-m to 1.5-km depth is in the northern portion of the study area. We interpret this increase in resistivity to be related to an increase in permeability, suggesting that the southern portion of the study area may be less permeable near the southern margin of the Silent Canyon caldera complex.

The geologic interpretations of the Calico Hills zeolitic composite unit in the resistivity model are not well determined where conductive Calico Hills zeolitic composite unit overlies conductive Bullfrog confining unit or where resistive lower permeabilities dominate. The geologic interpretations presented also increase in uncertainty with increasing depth from lack of well control at depth and the larger volumes of Earth averaged in the resistivity model with depth.

Future collection of magnetotelluric data in areas without any well control should wait until a higher resolution magnetotelluric survey with more closely spaced stations (for example, 100-m station spacing or less) near well control is proven effective at delineating these confining units with a satisfactory degree of confidence.

Acknowledgments

The three-dimensional resistivity model was originally constructed and inverted by Erin Wallin, formally with the U.S. Geological Survey and currently with GNS Science, Avalon, Lower Hutt, New Zealand. The magnetotelluric data were collected by U.S. Geological Survey scientists Beth Burton and Jackie Williams (retired). Helpful comments and suggested revisions were provided by Ted Asch, U.S. Geological Survey, and Lance Prothro, National Security Technologies, LLC.

References Cited

Bechtel Nevada, 2002, A hydrostratigraphic model and alternatives for the groundwater flow and contaminant transport model of Corrective Action Units 101 and 102—Central and western Pahute Mesa, Nye County, Nevada: U.S. Department of Energy Report DOE/NV /11718–706, 383 p.

Bechtel Nevada, 2005, A hydrostratigraphic framework model and alternatives for the groundwater flow and contaminant transport model of corrective action unit 98: Frenchman Flat, Clark, Lincoln and Nye Counties, Nevada: U.S. Department of Energy DOE/NV/11718–1064, 240 p.

Bechtel Nevada, 2006, A hydrostratigraphic model and alternatives for the groundwater flow and contaminant transport model of Corrective Action Unit 97—Yucca Flat–Climax Mine, Lincoln and Nye Counties, Nevada: U.S. Department of Energy Report DOE/NV/11718–1119, 288 p.

Bendat, J.S., and Piersol, A.G., 1971, Random data: analysis and measurement procedures: New York, Wiley Interscience, 407 p.
Blankennagel, R.K., and Weir, J.E., Jr., 1973, Geohydrology of the eastern part of Pahute Mesa, Nevada Test Site, Nye County, Nevada: U.S. Geological Survey Professional Paper 712–B, 35 p.
Byers, F.M., Jr., Carr, W.J., Christiansen, R.L., Lipman, P.W., Orkild, P.P., and Quinlivan, W.D., 1976a, Geologic map of the Timber Mountain caldera area, Nye County, Nevada: U.S. Geological Survey Miscellaneous Investigations Series Map I–891, scale 1:48,000, 10 p.
Byers, F.M., Jr., Carr, W.J., Orkild, P.P., Quinlivan, W.D., and Sargent, K.A., 1976b, Volcanic suites and related cauldrons of the Timber Mountain-Oasis Valley caldera complex, southern Nevada: U.S. Geological Survey Professional Paper 919, 70 p.
Byers, F.M., Jr., Carr, W.J., and Orkild, P.P., 1989, Volcanic centers of southwestern Nevada—Evolution of understanding, 1960–1988: Journal of Geophysical Research, v. 94, p. 5908–5924.
Carr, W.J., Byers, F.J., Jr., and Orkild, P.P., 1986, Stratigraphic and volcano-tectonic relations of Crater Flat Tuff and some older volcanic units, Nye County, Nevada: U.S. Geological Survey Professional Paper 1323, 28 p.
Dickerson, R.P., and Drake, R.M. II, 1998, Geologic map of the Paintbrush Canyon area, Yucca Mountain, Nevada: U.S. Geological Survey Open-File Report 97-783, scale 1:6,000, 25 p. text.
Dobrin, M.D., and Savit, C.H., 1988, Introduction to geophysical prospecting (4th ed.): New York, McGraw-Hill, 867 p.
DOE UGTA, 2003, Underground test area fact sheet: DOE/NV-915, August 2003.
Eberhart-Phillips, Donna, Stanley, W.D., Rodriguez, B.D., and Lutter, W.J., 1995, Surface seismic and electrical methods to detect fluids related to faulting: Journal of Geophysical Research, v. 100, no.B7, p. 12919–12936.
EMI, Inc., 1996, MT-1 magnetotelluric system operation manual, version 3.2: Richmond, Calif., Electromagnetic Instruments, Inc., 220 p.
Faunt, C.C., Sweetkind, D.S., and Belcher, W.R., 2004, Three-dimensional hydrogeologic framework model, chap. E *of* Belcher, W.R., ed., Death Valley regional ground-water flow system, Nevada and California—Hydrogeologic framework and transient ground-water flow model: U.S. Geological Survey Scientific Investigations Report 2004–5205, p. 165–256.
Ferguson, J.F., Cogbill, A.H., and Warren, R.G., 1994, A geophysical-geological transect of the Silent Canyon caldera complex, Pahute Mesa, Nevada: Journal of Geophysical Research, v. 99, p. 4323–4339.
Gamble, T.D., Goubau, W.M., and Clarke, J., 1979, Error analysis for remote reference magnetotellurics: Geophysics, v. 44, no. 5, p. 959–968.
Geldon, A.L., 2004, Hydraulic tests of Miocene volcanic rocks at Yucca Mountain and Pahute Mesa and implications for groundwater flow in the southwest Nevada volcanic field, Nevada and California: Geological Society of America Special Paper, v. 381, 93 p.
Geosystem, 2007, WinGLink® User's Guide, Release 2.20.01: Milan, Italy, 469 p.
Hallenburg, J.K., 1998, Non-hydrocarbon methods of geophysical formation evaluation: Boca Raton, Fla, Lewis Publ., 265 p.
Hearst, J.R., and Nelson, P.H., 1985, Well logging for physical properties: New York, McGraw-Hill Book Co., 571 p.
Hearst, J.R., Nelson, P.H., and Paillet, F.L., 2000, Well logging for physical properties, 2nd edition: New York, John Wiley & Sons, 483 p.
IT Corporation, 1996, Underground test area subproject phase I data analysis task (Vol. I)-Regional geologic model data documentation package: Las Vegas, Nev., ITLV/10972-81, 407 p.

Kaufman, A.A., and Keller, G.V., 1981, The magnetotelluric sounding method, *in* Methods in geochemistry and geophysics, 15: Amsterdam, Elsevier Scientific Publishing Company, 595 p.
Keller, G.V., 1987, Rock and mineral properties, *in* Nabighian, M.N., ed., Electromagnetic methods in applied geophysics theory: Tulsa, Okla., Society of Exploration Geophysicists, v. 1, p. 13–51.
Keller, G.V., 1989, Electrical properties, *in* Carmichael, R.S., ed., Practical handbook of physical properties of rocks and minerals: Boca Raton, Fla., CRC Press, p. 359–427.
Keller G.V., Frischknecht F.C., 1966. Electrical methods in geophysical prospecting: Oxford, Pergamon Press, Inc., 519 p.
Laczniak, R.J., Cole, J.C., Sawyer, D.A., and Trudeau, D.A., 1996, Summary of hydrogeologic controls on groundwater flow at the Nevada Test Site, Nye County, Nevada: U.S. Geological Survey Water-Resources Investigations Report 96–4109, 59 p.
Mackie, R.L., Madden, T.R., and Wannamaker, P.E., 1993, Three-dimensional magnetotelluric modeling using difference equations; theory and comparisons to integral equation solutions: Geophysics, v. 58, no. 2, p. 215–226.
Mackie, R.L., Smith, J.T., and Madden, T.R., 1994, Three-dimensional electromagnetic modeling using finite difference equations: the magnetotelluric example: Radio Sci., v. 29, p. 923–935.
Moyer, T.C., and Geslin, J.K., 1995, Lithostratigraphy of the Calico Hills Formation and the Prow Pass Tuff (Crater Flat Group) at Yucca Mountain, Nevada: U.S. Geological Survey Open–File Report 94–460, 59 p.
National Security Technologies, LLC, 2007, A hydrostratigraphic model and alternatives for the groundwater flow and contaminant transport model of Corrective Action Unit 99—Rainier Mesa–Shoshone Mountain, Nye County, Nevada: U.S. Department of Energy Report DOE/NV/25946-146, 302 p.
Nelson, P.H., and Anderson, L.A., 1992, Physical properties of ash flow tuff from Yucca Mountain, Nevada: Journal of Geophysical Research, v. 97, no. B5, p. 823–841.
Palacky, G.J., 1987, Resistivity characteristics of geologic targets, *in* Nabighian, M.N., ed., Electromagnetic methods in applied geophysics: Tulsa, Okla., Society of Exploration Geophysicists, v. 1, p. 53–129.
Prothro, L.B., and Drellack, S.L., Jr., 1997, Nature and extent of lava-flow aquifers beneath Pahute Mesa, Nevada Test Site: Las Vegas, Nev., Report DOV/NV/11718-156 prepared for the U.S. Department of Energy, National Nuclear Security Administration Nevada Site Office by Bechtel Nevada, 50 p.
Reddy, I.K., Rankin, David, and Phillips, R.J., 1977, Three-dimensional modelling in magnetotelluric and magnetic variational sounding: Geophysics Journal of the Royal Astronomical Society, v. 51, p. 313–325.
Sawyer, D.A., Fleck, R.J., Lanphere, M.A., Warren, R.G., Broxton, D.E., and Hudson, M.R., 1994, Episodic caldera volcanism in the Miocene southwestern Nevada volcanic field—Revised stratigraphic framework, 40Ar/39Ar geochronology, and implications for magmatism and extension: Geological Society of America Bulletin, v. 106, p. 1304–1318.
Siripunvaraporn, W., Egbert, G., Lenbury, Y., and Uyeshima, M., 2005, Three-dimensional magnetotelluric inversion: data space method: Physics of the Earth and Planetary Interiors, v. 150, no. 1–3, p. 3–14.
Sternberg, B.K., Washburne, J.C., and Pellerin, Louise, 1988, Correction for the static shift in magnetotellurics using transient electromagnetic soundings: Geophysics, v. 53, p. 1459–1468.
Sweetkind, D.S., Belcher, W.R., Faunt, C.C., and Potter, C.J., 2004, Geology and hydrogeology, *in* Belcher, W.R., ed., Death Valley regional groundwater flow system, Nevada and California–

Hydrogeologic framework and transient groundwater flow model: U.S. Geological Survey Scientific Investigations Report 2004–5205, p. 21.
Vozoff, Keeva, 1972, The magnetotelluric method in the exploration of sedimentary basins: Geophysics, v. 37, p. 980–141.
Vozoff, Keeva, 1991, The magnetotelluric method, *in* Nabighian, M.N., ed., Electromagnetic methods in applied geophysics: Tulsa, Okla., Society of Exploration Geophysicists, v. 2, pt. B, p. 641–711.
Wannamaker, P.E., Hohmann, G.W., and Ward, S.H., 1984, Magnetotelluric responses of three-dimensional bodies in layered earths: Geophysics, v. 49, no. 9, p. 1517–1533.
Winograd, I.J., and Thordarson, W., 1975, Hydrogeologic and hydrochemical framework, south-central Great Basin, Nevada-California, with special reference to the Nevada Test Site: U.S. Geological Survey Professional Paper 712–C, 126 p.

Appendix A. Three-Dimensional Resistivity Model Depth Slices

Appendix A contains the three-dimensional (3-D) resistivity-model depth slices plotted from Geosystem's (2007) WinGLink 3-D Forward Modeling module, MT_4. Black inverted triangles are magnetotelluric stations. Distance scales are kilometers from XY mesh origin.

Appendix B. Three-Dimensional Resistivity Model East-West Cross Sections

Appendix B contains the three-dimensional (3-D) resistivity model east-west cross sections plotted from Geosystem's (2007) WinGLink 3-D Forward Modeling module, MT_4. Depth scale is positive depth (not negative depth, as shown) from model surface datum. Black numbered dots at surface are magnetotelluric stations. Distance scale is kilometers from XY mesh origin. West is negative distance. East is positive distance.

Appendix C. Three-Dimensional Resistivity Model North-South Cross Sections

Appendix C contains the three-dimensional (3-D) resistivity model north-south cross sections plotted from Geosystem's (2007) WinGLink 3-D Forward Modeling module, MT_4. Depth scale is positive depth (not negative depth, as shown) from model surface datum. Black numbered dots at surface are magnetotelluric stations. Distance scale is kilometers from XY mesh origin. North is negative distance. South is positive distance.

Appendix D. Three-Dimensional Resistivity Model Computed Apparent Resistivity and Phase

Appendix D contains the three-dimensional (3-D) resistivity computed apparent resistivity and phase curves overlaid on the observed apparent resistivity and phase data for each magnetotelluric station plotted from Geosystem's (2007) WinGLink Basic Processing module, MT_1. App Rho is apparent resistivity. Red and blue lines are the 3-D computed XY and YX apparent resistivity and phase curves, respectively.

Appendix E. Three-Dimensional Resistivity Inversion Depth Slices

Appendix E contains the three-dimensional (3-D) resistivity inversion depth slices plotted from Siripunvaraporn's (2005) 3-D inversion program for magnetotelluric data, WSINV3DMT. Black numbered dots are magnetotelluric stations. Distance scales are kilometers from XY mesh origin.

Appendix F. Three-Dimensional Resistivity Inversion East-West Cross Sections

Appendix F contains the three-dimensional (3-D) resistivity inversion east-west cross sections plotted from Siripunvaraporn's (2005) 3-D inversion program for magnetotelluric data, WSINV3DMT. Depth scale is positive depth (not negative depth, as shown) from model surface datum. Black numbered dots at surface are magnetotelluric stations. Distance scale is kilometers from XY mesh origin. West (W) is negative distance. East (E) is positive distance.

Appendix G. Three-Dimensional Resistivity Inversion North-South Cross Sections

Appendix G contains the three-dimensional (3-D) resistivity inversion north-south cross sections plotted from Siripunvaraporn's (2005) 3-D inversion program for magnetotelluric data, WSINV3DMT. Depth scale is positive depth (not negative depth, as shown) from model surface datum. Black numbered dots at surface are magnetotelluric stations. Distance scale is kilometers from XY mesh origin. North (N) is negative distance. South (S) is positive distance.

Appendix H. Three-Dimensional Resistivity Inversion Computed Apparent Resistivity and Phase

Appendix H contains the three-dimensional (3-D) resistivity inversion computed apparent resistivity and phase curves overlaid on the observed apparent resistivity and phase data for each magnetotelluric station plotted from Geosystem's (2007) WinGLink Basic Processing module, MT_1. App Rho is apparent resistivity. Red and blue lines are the 3-D computed XY and YX apparent resistivity and phase curves, respectively.

Appendix I. Magnetotelluric Data Plots

The figures in appendix H represent the field-processed magnetotelluric data for each station, after the time-series data were converted to the frequency domain and the tensor-transfer function was developed. Refer to the "Magnetotelluric Data" section in this report for an explanation of this processing. There are eight separate magnetotelluric data parameter plots for each station plotted from EMI's (1996) magnetotelluric data processing program, MTR15:

1. Apparent resistivity for the x-y direction (x symbol) and y-x direction (o symbol) modes
2. Impedance phase for the x-y direction (x symbol) and y-x direction (o symbol) modes
3. Impedance skew for the impedance tensor
4. Multiple coherency for the x-y direction (x symbol) and y-x direction (o symbol) modes of the electric field
5. Impedance polar plots (at 12 selected frequencies)
6. Tipper magnitude for the vertical magnetic field
7. Tipper strike for the vertical magnetic field
8. HzHx (x symbol) and HzHy (o symbol) Coherency

Error bars (],[) on the apparent resistivity, impedance phase, skew, tipper magnitude, and tipper strike plots represent probable errors within one standard deviation of the sample variance (Gamble and others, 1979).

Apparent resistivity is the approximate ratio of the electric-field strength to the magnetic-field strength at a given frequency. The impedance phase is proportional to the slope of the apparent resistivity curve on a log-log plot, but from baselines at ±45 degrees (Vozoff, 1991). A measure of the dimensionality for magnetotelluric data is provided by the impedance skew of the impedance tensor (Vozoff, 1972). If the effective measured resistivity response to the geology beneath a magnetotelluric station truly is one or two dimensional, then the skew will be zero. Instrumental and environmental sources of electrical noise can cause nonzero skew values. Skew values typically are small (about 0.1) for relatively low-noise recordings. Higher skews (above 0.2) are an indication of either the resistivity response to 3-D geology or higher levels of noise. Manmade electrical noise, such as power lines, power generators, and moving vehicles and trains, can have a negative effect on magnetotelluric data quality. All of these local disturbances can produce incoherent noise that mainly affects frequencies above 1 Hz. Other manmade electrical noise, such as direct-current electric trains and active cathodic protection of pipelines, produces coherent electromagnetic signals that mainly affect frequencies below 1 Hz.

The effects of near-surface resistivity anomalies can cause what are known as "static shifts" in the data (Sternberg and others, 1988). Cultural features also can affect the measured magnetotelluric responses. These features include fences, pipelines, communication lines, railways, and other manmade conductors.

In the survey area, noise from small power lines and small moving vehicles was negligible at distances greater than 0.4 km from the noise source. Powerline signal levels were measured at each site and were typically less than 20 percent of the maximum recordable signals. Noise from larger power

lines, power generators, pipelines, and trains was negligible at distances greater than 5 km. Local lightning, wind, and rainstorms may also degrade data quality. Burying the magnetic induction coils and the electric dipole wires minimized wind noise.

Predicted values of the electric field can be computed from the measured values of the magnetic field (Vozoff, 1991). The coherence of the predicted electric field with the measured electric field is a measure of the signal-to-noise ratio provided in the multiple coherency plots. Values are normalized between 0 and 1; values at 0.5 signify signal levels equal to noise levels. For this data set, coherencies were generally at an acceptable level, except at times in the frequency ranges of about 0.1 to 5 Hz (traditionally referred to as the "dead band").

The field-processed magnetotelluric data include some scatter and poor signal-to-noise ratios. Spectral results were inspected visually for noisy data, and the best signal-to-noise field data were combined into the final plots.

The magnetotelluric impedance polar plots provide a measure of magnetotelluric data dimensionality (Reddy and others, 1977). For 1-D resistivity structures, the principal impedance polar diagram (dashed line) is a circle. For 2-D or 3-D resistivity structures, the principal impedance polar diagram (dashed line) elongates either parallel or perpendicular to strike direction. Over resistors, the principal impedance polar diagram elongates perpendicular to strike direction, and over conductors, it elongates parallel to strike direction. For 2-D resistivity structures, the additional impedance polar diagram (solid line) attains the shape of a symmetric clover leaf. For 3-D resistivity structures, the additional impedance polar diagram (solid line) elongates in one direction, and its amplitude is comparable to that of the principal impedance polar diagram (dashed line).

The magnetotelluric "tipper" is calculated from the vertical component of the magnetic field. The tipper magnitude is a measure of the "tipping" of the magnetic field out of the horizontal plane (Vozoff, 1991). It will equal zero for the 1-D case. Typically, tipper value increases from 0.1 to 0.5 and seldom approaches 1, as it responds primarily to vertical and sub-vertical structures. The tipper strike is used to help resolve the 90-degree ambiguity in the impedance rotation angle. The HzHx and HzHy coherency is a measure of the signal-to-noise ratio of the vertical magnetic field with respect to each of the orthogonal, horizontal magnetic-field directions. Values are normalized between 0 and 1; values at 0.5 signify signal levels equal to noise levels. These three-component magnetic-field coherencies provide a check on the signal-to-noise ratio of the measured values in the tipper magnitude and tipper strike plots.